Memorandum M-721

Fatigue strength of riveted lap joints in GLARE 3 3/2-0.3 reduced-scale barrel, curved panel and flat panel design

(BE2040 subtask 6.1)
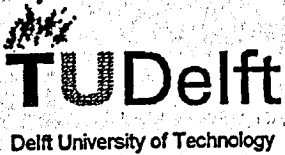
R.P.G. Müller, E. Holleman

TUDelft
Delft University of Technology

Faculty of Aerospace Engineering
Structures and Materials Laboratory
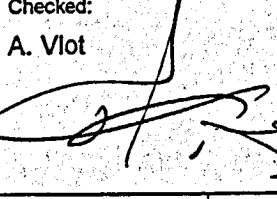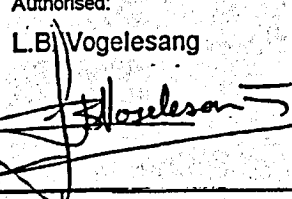
Publisher: Delft University of Technology
Faculty of Aerospace Engineering
Structures & Materials Laboratory
P.O. Box 5058
2600 GB Delft
The Netherlands.

Memorandum M-721

Faculty of Aerospace Engineering

TUDelft

Delft University of Technology

Kluyverweg 1
2629 HS Delft
The Netherlands

Structures & Materials Laboratory

Project:	Brite Euram 2040 (BE2040)	Project Duration:
Project Title:	Fibre Metal Laminate and CFRP Fuselage Concepts	1.11.92 - 1.11.95

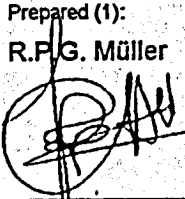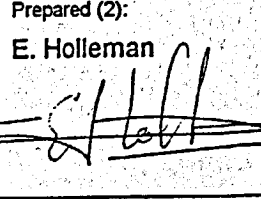|	
Document Number:	Memorandum M-721
Title and Subtitle:	Fatigue strength of riveted lap joints in GLARE 3 3/2-0.3 reduced-scale barrel, curved panel and flat panel design (BE2040 subtask 6.1)
Author(s):	R.P.G. Müller, E. Holleman
Date:	30 October 1995

Abstract:

—This document focuses on the fatigue behaviour of reduced-scale barrels, curved panels and flat panels. Two types of skin material, namely GLARE 3 3/2-0.3 and 2024-T3 clad, are investigated. The significance of coupon tests for the fatigue behaviour of a riveted lap joint in a fuselage is evaluated. Special attention is paid to the behaviour of reduced-scale barrel specimens in comparison to flat specimens. Differences between flat coupons and fuselages are discussed based on calculations and experiments.

The research covers in-house work and work carried out in the scope of subtask 6.1 of the BE2040 work program.

Keywords:	Security class:
—GLARE 3 3/2-0.3, fatigue, lap joint, rivet squeeze force, reduced-scale barrel, curved panel, flat panel, full-scale barrel	Unrestricted

Prepared (1):	Prepared (2):	Checked:	Authorised:
R.P.G. Müller	E. Holleman	A. Vlot	L.B. Vogelesang

TU Delft code:	Issue number:	Issue date:	Total of pages:	First issue:	BE2040 code:
M-721	1	30.10.95	66	30.10.95	BE2040-B-

DISTRIBUTION LIST

BE2040 partners:

1.	Structural Laminates BV	J.W. Gunnink
2.	Structural Laminates BV	B. van Wimersma Greidanus
3.	Structural Laminates BV	A.C. Mattousch
4.	Fokker Aircraft	L.H. van Veggel
5.	Fokker Aircraft	J. Homan
6.	Daimler Benz Aerospace Airbus	W.D. Dolzinski
7.	BAe Airbus	J. Ball
8.	Aerospatiale	B. Béral
9.	Aermacchi	S. Pievani
10.	Alenia Mase	G. Vanucchi
11.	CASA	M.A. Morell
12.	Dornier Luftfahrt GmbH	K.F. Sahm
13.	Dassault Aviation	P. Vautey
14.	Daimler Benz Central Laboratories	K. Drechsler
15.	DLR	K.H. Trautmann
16.	DRA	P. Poole
17.	NLR	W. v.d. Hoeven
18.	Inasco	D. Bofilios
19.	TU Braunschweig	R. Kickert

Internal distribution:

20.	L.B. Vogelesang	B2
21.	J. Schijve	B2
22.	A. Vlot	B2
23.	J. Sinke	B2
24.	T. J. van Baten	B2
25.	R.P.G. Müller	B2
26.	E. Holleman	B2
27.	Library	B2
28-33.	Faculty of Aerospace Engineering	

CONTENTS

NOTATIONS

Symbol	Unit	Description
c	mm	Difference between sheet thickness and countersink depth.
d	mm	Rivet diameter.
D_0	MPa	Initial rivet diameter.
E	kN	Young's modulus.
F_{sq}	mm	Squeeze force.
h	mm	Countersink depth.
K_t	MPa√m	Stress intensity factor.
L	–	Longitudinal direction
Δp	MPa	Differential pressure.
p	mm	Rivet pitch.
R	mm	Radius.
R	–	Stress ratio.
ΔR	mm	Radial expansion.
s	mm	Row pitch.
t	mm	Sheet thickness
δ	mm	Rivet head protrusion relative to sheet surface.
ϵ	%	Strain.
ν	–	Poisson's ratio.
χ	–	Biaxiality ratio.
σ	MPa	Applied stress.
σ	MPa	Nominal stress.

1   INTRODUCTION

1.1   General

Within the scope of the European Fuselage Program (Brite Euram project BE2040 [ref.1]) and in-house research on lap joint fatigue, Delft University of Technology has investigated the fatigue strength of riveted lap joints in reduced-scale barrel, curved panel and flat panel design. Subtask 4.1 (Development of Building Blocks for Fibre Metal Laminates) covers the program definitions and the production of test specimens [ref. 2]. The results of subtask 4.1 are evaluated through testing of longitudinal lap joints in subtask 6.1 (Testing of Fibre Metal Laminate Building Blocks). This report contains the results of the in-house program as presented in [ref. 3] and the results of the experimental work agreed within the scope of the BE2040 program.

The objective is to compare reduced-scale barrels, curved panels and flat panels in terms of fatigue performance. Two types of skin material, namely GLARE 3 3/2-0.3 and 2024-T3 clad, are investigated. A schematic illustration of a GLARE 3 3/2 lay-up together with an overview of standardised GLARE configurations is shown in appendix A. The significance of coupon tests for the fatigue behaviour of a riveted lap joint in a fuselage is evaluated. Special attention is paid to the behaviour of reduced-scale barrel specimens in comparison to flat specimens. Differences between flat coupons and fuselages are discussed based on calculations and experiments.

1.2   Outline of the research

There is a significant discrepancy between fuselage and flat coupon fatigue behaviour. From [ref. 3] it can be deduced that:

- the fatigue life of a simple lap joint coupon, tested under laboratory conditions and similar nominal hoop stress, may be 5 times higher than the fuselage fatigue life.
- the fatigue stress on the specimen should be approximately 1.2 times higher than the nominal stress in the fuselage skin to obtain a comparable fatigue life.

This discrepancy in fatigue behaviour is principally due to the fact that the complex loading conditions of the fuselage, i.e. biaxiality, pillowing and bending, are not accounted for. Other aspects, like secondary bending, are not similar and further enhance the difference in fatigue performance between coupon and fuselage [ref. 3]. To evaluate the influence of several of these aspects, the following issues are considered.

<u>Analytical and FE calculations</u>
Deflections of fuselage skins with and without frames are calculated analytically. The more complex behaviour of riveted joints in pressurised (stiffened) fuselage sections is investigated by use of 2-d and 3-d FE models.

Flat specimens

Flat panels are tested uniaxially and evaluated in terms of fatigue behaviour. In addition, a test set-up is developed in which lap joints are loaded biaxially. The connections of the specimen to the rigs is performed with fibres to avoid restraint of stiff clamps.

Curved panels

A test set-up developed by Chen [ref. 4] is used to investigate the effect of curvature and internal pressurisation for the fatigue life of riveted lap joints. The specimen is loaded uniaxially by internal pressure.

Reduced-scale barrels

The test set-up has two rigid bulkheads, which enables investigation of the contribution of frames for pillowing and hoop stress reduction. The cylindrical specimen is loaded biaxially by compressed air. Fuselage bending effects are not accounted for. The mechanical behaviour of riveted lap joints is investigated and compared to analytical results. The fatigue behaviour is investigated under biaxial pressure conditions.

Section 2 covers FE calculations and verification measurements. In section 3 the fatigue test results are evaluated.

2   TEST PROGRAM

2.1   Materials

Two types of skin material, namely GLARE 3 3/2-0.3 and 2024-T3 clad, are investigated. The nominal thickness of the 2024-T3 sheets is 1.0 mm. The GLARE laminate (nominal thickness 1.42 mm) is a standard production material build up of chromic acid anodised aluminium layers with bare surfaces. Blanks are taken from several production batches (batch numbers unknown).

2.2   Specimens and test set-up

Two types of lap joint geometry are investigated: one has 4.0 mm NAS1097AD flush head rivets equally placed at a rivet pitch, p, and row pitch, s, of 20 mm, the second type contains 4.8 mm NAS1097DD flush head rivets with p and s equal to 24 mm. The lap joints have three rows of rivets. The aluminium rolling direction is parallel to the lap joint orientation (L-direction).
Rivet hole preparation is done using a table mounted drill device and HSS drills. Standard tools are used to countersink the holes. The rivets are installed using a constant squeeze force level of 14 kN for the 4.0 mm rivets and 22 kN for the 4.8 mm rivets. For this purpose, a computer controlled riveting device has been developed by the Structures and Materials Laboratory. All specimens are dry assembled.

Reduced-scale barrel specimens
Four cylinders are tested: three 2024-T3 cylinders and one GLARE 3 3/2-0.3 cylinder. A schematic illustration of the specimen configuration is shown in figure 2.1. The barrel radius is 613 mm, the barrel length is 500 mm (effective length is 420 mm) and the biaxiality ratio χ is 0.5 (beyond the frames). A photograph of the test set-up is shown in figure 2.2. Each cylinder contains four longitudinal riveted lap joints, spaced at 90°. Three lap joints are riveted under constant squeeze force. The fourth joint, which is the closing joint, is riveted in the barrel test set-up using a hand rivet gun. This joint has four rows of protruding head rivets in order to prevent preliminary fatigue failure.

The GLARE barrel has two lap joints with 4.0 mm rivets and one with 4.8 mm rivets. For the 2024-T3 barrels only 4.0 mm rivets are used. The 4.0 mm rivets in both 2024-T3 and GLARE 3 are not fully flushed, they protrude 0.1 mm above the sheet surface.

Two methods of sheet preparation are applied. The sheets for two 2024-T3 barrels are first riveted, subsequently mounted in the test set-up and elastically bent to adapt the barrel radius. The sheets for the third 2024-T3 barrel are roll-formed, except for 10 mm of the edges, to the required barrel radius. The first method of sheet preparation introduces built in stresses, the second residual stresses due to plastic deformation. The fatigue behaviour of the three barrels is compared to investigate the effect of sheet preparation.

The sheets for the GLARE barrel are roll-formed including the 10 mm edges to the desired curvature.

In view of preventing fatigue failures at the skin connections to the heavy steel pressure bulkheads, the cylinder ends are provided with bonded doublers. Suitable dimensions of the doublers have been obtained by FE calculations.

Curved panel specimens
The PFSTS (Pressurised Fuselage Skin Test System) set-up shown in the figures 2.3 and 2.4 has been developed to investigate crack edge bulging, a typical phenomenon for curved sheet specimens loaded by internal pressure [ref. 4]. The specimens measure 500 mm by 1080 mm and have a 2000 mm radius of curvature. The specimens are loaded uniaxially by internal pressure. The biaxiality ratio χ is zero.
A flat, riveted lap joint specimen is mounted in the test set-up and elastically bent to adapt the set-up curvature. Since the specimen is not connected to a bulkhead, there is a free radial expansion. Except for the edge rivets, all other rivets are loaded by the same membrane and bending stress. Additional edge rivets are installed to reduce the secondary bending at the specimen edges in order to prevent premature failure because of edge effects [ref. 3].

Three specimens are tested: two 1.0 mm 2024-T3 clad and one GLARE 3 3/2-0.3. The lap joint configurations are similar for both materials and contain 4.0 mm rivets.

Flat panel specimens
The specimen geometry is shown in figure 2.5. Two 2024-T3 lap joints and one GLARE 3 lap joint, all three assembled with 4.0 mm rivets, are tested. Steel blocks are attached to the specimen edges (figure 2.6) to reduce secondary bending at these locations and consequently preventing fatigue crack initiation at the edge rivets.

2.3   Test procedure

All fatigue tests are performed under a room temperature test environment. The maximum applied stress in the undisturbed skin area is 97 MPa for 2024-T3 and 124 MPa for GLARE 3 3/2-0.3. For the curved specimens, the corresponding levels of internal pressure Δp are 0.0485 MPa for 2024-T3 and 0.0868 MPa for GLARE 3. The corresponding Δp for the reduced-scale barrels is 0.1582 MPa for 2024-T3 and 0.2832 MPa for GLARE 3. The stress ratio R is 0.02 for GLARE 3 and 0.03 for 2024-T3. Frequency of testing is 0.07 Hz for the barrels, 0.1 Hz for the curved specimens and 5 Hz for the flat specimens.

During testing, the 2024-T3 lap joints are inspected visually by use of an optical microscope. To detect small cracks and subsurface cracks in the GLARE 3 lap joints the Nortec 19e Eddyscope is used. This device enables the detection of cracks with a length of 0.5 mm in the third aluminium layer subsurface [ref. 5]. At the start of the fatigue test,

the eddy current response of each critical rivet location is stored in the memory of the Eddyscope, then small crack indications will not remain undetected in the rivet response scatter.

For GLARE 3 3/2-0.3 (figure 2.7) cracks in the surface aluminium layers (layers 3) can be detected with the Nortec SPO sliding probe operated at a frequency of 9 kHz. The location of the sliding probe on the specimen should be reproducible to have unique responses. For this purpose, lines are drawn on the sheet surface to position the ruler along which the probe is guided. The location of the sliding probe should be adjusted to the crack initiation location. For the GLARE 3 configuration investigated a sliding probe location at 1 mm distance from the net section in the direction of the clamps (figure 2.8) provides satisfactory results. The middle aluminium layers (layers 2) are inspected by use of a pencil probe with a 3 mm diameter and operated at 50 kHz. The inner aluminium layers (layers 1) are inspected with the same pencil probe at a frequency of 300 kHz.

Reduced-scale barrels

Before fatigue testing, deflection measurements are performed by use of a linear voltage displacement transducer (LVDT), which is in contact with the sheet outer surface (see figure 2.9). The out-of-plane displacement is scanned along vertical lines in longitudinal direction. The LVDT is attached to a servo-hydraulic frame allowing contour scans in circumferential direction. The displacement transducer has its radius reference point on the pressure bulkheads.

2.4 Additional remarks

The use of a 4.0 mm flush head rivet in 1.0 mm 2024-T3 sheet provides a knife-edge condition, as illustrated in figure 2.10. In metal sheets a knife-edge is not allowed mainly because the underlying sheet is also countersunk yielding lower static and fatigue strength (K_t increases). When installing the rivets force-controlled instead of translation-controlled, i.e. not the driven head geometry but the squeeze force is the rivet parameter, this knife-edge condition may be allowed provided a high squeeze force is applied. From [ref. 3] the following results are deduced.

Fatigue tests on anti-symmetric two-row lap joints have been performed. The critical rows of these lap joints, schematically shown in figure 2.11, have either only countersunk holes (type I) or non-countersunk holes (type II). The advantage of this type of specimen is that fatigue cracking will occur at both end rows, provided the rivets are equally squeezed and no imperfections are present. The results of figure 2.12 show that the top row configuration (i.e. the countersunk holes) is critical for the full range of squeeze forces. Despite the knife-edge condition, still a significant life improvement of the countersunk configuration for higher squeeze forces is obtained. It does not perform significantly worse than the non-countersunk configuration. The hole expansions are large close to the faying surface introducing residual stresses which are favourable from a fatigue point of view.

Hole expansion and residual stress depend on the geometric ratio of sheet thickness to rivet diameter. Therefore, specimens with different t/D_0 ratios have been tested for a range of rivet squeeze forces (5 kN to 41 kN). For identical rivet diameters equal squeeze forces are used irrespective of the sheet thickness. In addition, specimens were prepared to have equal driven head dimensions of 1.2, 1.5 and 1.75 times the original shank diameter. Knife-edge requirements have been ignored to investigate a large range of t/D_0 ratios. To separate the contributions of the squeeze force for the fatigue performance of the bottom row and top row, the anti-symmetric lap joints of figure 2.11 are used. The test results are shown in figure 2.13. The difference in fatigue behaviour of the two types of lap joint are small at low squeeze force. The fatigue life of the non-countersunk configuration (type II) can be three times higher than that of the countersunk (type I), although the difference mainly depends on the sheet thickness. Lap joint type I with the critical countersunk rows demonstrates less increase in fatigue life at higher squeeze forces.

The fatigue lives for constant sheet thickness of the critical countersunk end rows are presented in figure 2.14 for given driven head dimensions. The fatigue performance of 1.0 mm 2024-T3 (two-row) lap joints with (4.0 mm rivets, c is 0 mm) and without (3.2 mm rivets, c is 0.25 mm) knife-edge condition is considered. Test data of 1.6 mm 2024-T3 lap joints are included. In particular at high squeeze force, the larger rivet diameter is superior to the smaller diameter. At low squeeze force the difference in bearing load is small due to the relatively small contact area. Apparently for high levels of squeeze force the residual stresses because of squeezing become favourable. Because the top row in a conventional riveted joint is critical, a higher squeeze force should be chosen, particularly for thin sheets.

Figure 2.15 provides some joint ultimate strength data determined by single-lap joint shear testing.

As shown by the test results, the effect of knife-edge on fatigue and static strength reduces with increased squeeze force. At low squeeze force, the effect is significant, it reduces at moderate squeeze force while the effect is negligible at high squeeze force.

3   ANALYSIS OF FUSELAGE LAP JOINTS

3.1   Skin deformation

Unstiffened fuselage
The internal pressure (Δp) applied to an <u>unstiffened</u> fuselage yields the following stresses in the skin:

$$\sigma_{hoop} = \frac{\Delta p \cdot R}{t}$$

$$\sigma_{axial} = \frac{\Delta p \cdot R}{2t}$$

(3.1)

The stress in the axial direction of the fuselage (σ_{axial}) is half the stress in the circumferential direction (σ_{hoop}). The biaxiality ratio χ is 0.5. The strains in the skin can be derived with equation 3.1 and Hooke's law for plane stress:

$$\varepsilon_{hoop} = \frac{\Delta p \cdot R}{E \cdot t} \cdot \left\{ 1 - \frac{\nu}{2} \right\}$$

$$\varepsilon_{axial} = \frac{\Delta p \cdot R}{E \cdot t} \cdot \left\{ \frac{1}{2} - \nu \right\}$$

(3.2)

The hoop strain is approximately a factor of 4 larger than the axial strain. The radial expansion of the unstiffened cylinder is proportional to ε_{hoop}, which leads to:

$$\Delta R = \frac{\Delta p \cdot R^2}{E \cdot t} \cdot \left\{ 1 - \frac{\nu}{2} \right\}$$

(3.3)

Some illustrative values for an unstiffened aluminium fuselage are given in the table below. Values of t and Δp (cabin pressure) were chosen as characteristic values for the size of the fuselage (radius R).

Material	R [mm]	t [mm]	Δp [bar]	σ_{hoop} [MPa]	ΔR [mm]
2024-T3 clad	1500	1.0	0.5	75	1.4
	2000	1.2	0.52	86	2.1
	3000	1.6	0.574	108	3.9
GLARE 3 3/2-0.3	3000	1.4	0.574	116	5.0

When replacing aluminium by GLARE for the fuselage skin, the skin thickness can be reduced. Consequently, the radial deflection of the skin increases due to the larger hoop stress and lower Young's modulus both.

Fuselage with stiffeners and frames
Frames and stiffeners will restrain the radial expansion of the skin. Dependent of the stiffness of the frame-skin connection, the frames are loaded in the circumferential direction. At the same time, the frames will reduce the radial expansion of the skin and therefore the hoop stress. Hoop stress reductions can be in the order of 20 to 30% for a relative stiff frame skin connection, and in the order of 10% for a low stiffness skin/frame connection without crack stopper bands at the frames (floating frames).

The pillowing of the skin near the frames will result in bending stresses in axial direction of the skin. With infinitely stiff frames these bending stresses can become approximately 1.5 times the undisturbed hoop stress [ref. 6]. The radius of the cylinder and the sheet thickness largely determine the area, which is significantly affected by pillowing around the frames. An analytical solution is available for perfectly stiff frames if longitudinal stiffeners are not present. The length of the affected zone is approximately $3\sqrt{(Rt)}$ [ref. 7].
Radial expansion measurements have been performed on a GLARE 3 3/2-0.3 reduced-scale barrel. The results are shown in figure 3.1. The experimental results are in close agreement with the FE calculations. The difference between cylinders with and without doublers at the bulkheads is also obvious. The affected length of the cylinder is in the order of 75 mm.

Longitudinal stiffeners attached to the skin will further restrain the radial expansion. With stiff frames, a rigid frame/skin connections, and stiffeners with a high bending stiffness, double pillowing will occur, see figure 3.2. Skin bending will occur, but the hoop stress is reduced. To which extent frames and stiffeners affect the riveted lap joint stresses is discussed in section 3.3.

3.2   Unstiffened pressurised cylinder

It is well known that the stress distribution around an open hole for uniaxial loading and biaxial loading is significantly different. The K_t for an open hole in a large plate is equal to 3.0, whereas for an biaxiality ratio of 0.5 it is reduced to 2.5. The question is more problematic for a filled hole, with some hole/rivet interference, and for a pin-loaded hole. Moreover, in a riveted lap joint in a fuselage, the biaxiality could affect the load transfer distribution between the rivet rows and the secondary bending as well. In view of such a complex problem setting, there are two options: FE calculations and experiments. This section deals with FE calculations.
Two FE models are considered: (I) a 2-d model without considering effects of frames and stiffeners, and (ii) a 3-d model including the effect of frames. The results are discussed below.

2d-FE calculations

A 2-d FE model was developed for the calculation of secondary bending and rivet row load transmissions of a lap joint in a cylinder. There are no pressure bulkheads in the model. The 2d character implies that flat cross sections remain flat. The sheets are modelled with quadratic B22 beam elements and the rivets are represented as B21 beam elements [ref. 8]. Contact elements (GAPCYL [ref. 8]) are used at the overlap to prevent interference of the mating sheets. Biaxiality cannot be introduced and lateral contraction is ignored. To investigate the consequences of load biaxiality for a joint in an unstiffened cylinder a different model is used. The skin is represented by S8R sheet elements and the overlap is connected with B32 beam elements to represent the rivets [ref. 8]. At the overlap, contact elements (GAPCYL [ref. 8]) are used to prevent interference of the mating sheets. For this improved "2½-d" model, symmetry is used at the ends of the cylinder in axial direction. Similar to the 2-d model, part of the circumference (40-90°) is investigated and anti-symmetry is used at the ends in circumferential direction, which implies more joints present in the total 360°, see inset figure 3.3.

Results on radial deflections are presented in figure 3.3. Some analytical data is presented in appendix B. There is a different deflection for the top row and the bottom row sheet. The inner sheet rotates downwards, and the outer sheet inwards in order to bring the average neutral line deflection of the two sheets at the same radial deflection outside the overlap in the undisturbed sheet. It implies that the inner sheet expands more then the outer sheet, with a translation of the joint in circumferential direction towards the sheet with the larger expansion to maintain equal membrane stresses for the mating sheets. The radial deflections for the two biaxiality ratio's χ equal to 0.5 and 0 imply a similar deflection pattern of the overlap of the lap joint and are fully similar to those obtained in a uniaxially loaded flat lap joint specimen. In other words, it indicates that the sheet curvature does not affect the secondary bending.

Some additional information on secondary bending was obtained by strain gauge measurements on a flat biaxially loaded riveted lap joint (figure 3.4). The transverse load on the lap joint does not restrain the overlap rotation. Static experiments were carried out at different biaxiality ratio's. The results in figure 3.5 show a small effect of the biaxiality on the secondary bending, i.e. about a 5% reduction for χ equal to 0.5.

The 2-d FE calculations can also be used to analyse the distribution of the rivet row load transmission and secondary bending. However, it must be decided whether the internal pressure between the points A and B in figure 3.6 is applied on the unloaded free end of the inner sheet, or to the outer sheet. The first option should be adopted if a sealant is applied between the two sheets, which prevents the internal pressure to enter between the inner and the outer sheet. If this can not be prevented, the second option must be used. Calculations have been performed for both cases. The results in figure 3.7a show that the rivet row load distribution is slightly sensitive for pressure entrance between the two sheets. The secondary bending results in figure 3.7b indicate a significantly different

behaviour for the secondary bending. Actually, if there is pressure between the two sheets, the anti-symmetric configuration of the riveted lap joint is still maintained with respect to the internal pressure load. The same anti-symmetric configuration also applies to the uniaxially loaded flat lap joint specimen. However, this is no longer true if the pressure can not enter between the two sheets in the AB overlap. The anti-symmetry of the internal pressure application is lost. Although this phenomenon becomes less significant for larger cylinder radii, it does not disappear. The barrel tests discussed in section 3 have been carried out on specimens which have been assembled without using an interfaying sealant. For this reason, the 3-d FE calculations in general have been done for the symmetric internal pressure application.

3.3 Pressurised cylinder with frames

The deformation response of a longitudinal riveted lap joint in a pressurised cylinder with frames is different from the response of an unstiffened cylinder, discussed in the previous section. A 3d-FE model is required to make calculations if frames are present. In figure 3.8 an element distribution is presented for a riveted lap joint in a cylinder. When the 2½-d model is extended with restraint at the ends of the cylinder a 3-d model is obtained. The bulkhead is modelled by preventing displacements ($\Delta R = 0$) and rotations. For the radial displacement a multi-point constrained is used which allows a simulation of frames with different stiffness.

A displacement plot is presented in figure 3.9 for the circumferential location midway between the frames. The displacements are not disturbed by the frames. The radial displacement is different compared to the result for the unstiffened cylinder. The radial displacements of both sheets, away from the lap joint, are similar to the nominal radial deflection. The two sheets do not have the neutral lines at identical radii as it was found in the 2-d model for joints in unstiffened cylinders. In spite of this observation, differences between the bending deformations and stresses at the overlap could not be indicated. A quantitative comparison between the results of the 2-d and 3-d finite element models could not be made for the secondary bending stresses due to different modelling techniques of the rivets. The 3-d model gives a stress singularity in the sheet at the rivet locations. It prevents a stress investigation close to the rivet. However, if realistic fuselage skin deformations are required, frames should be included in the calculations.

Results of radial displacement measurements (ΔR) on a 2024 barrel are presented in figure 3.10 in comparison to calculated values. The experiments show the same trend as the calculations. The irregularities of the measurements are caused by imperfections of the skin.

Radial deflections have been calculated for a pressurised cylinder with and without biaxiality, see the results for χ is 0.5 and 0 in figure 3.11. The deflections are reduced by

the biaxiality as should be expected. However, the rotation of the overlap remains the same.

Load transfer and secondary bending in the critical row
The rigid frames in the reduced-scale barrel specimens at a frame spacing of 400 mm are causing a significant inhomogeneity of the load distribution along the rivet rows of the lap joints. The 3d-FE calculations show that lateral loads occur on the rivets near the two frames. In view of pillowing, such loads should be expected. However, the load transmission in the hoop stress direction is smaller than away from the frames. The practical significance of the lateral loads thus seems to be limited.

The rivet load distribution of the critical row between the frames is shown in figure 3.12a. Distributions have been calculated for different radii of curvature. The effect of the radius midway between the frames is rather small. However, the full restraint of the bulkhead results in more affected rivets for a larger radius of curvature. For the largest radius the restraint of the frame still results in smaller rivet loads midway between the frames compared to undisturbed load transfer.

Some interesting comments can now be made associated with the results of figure 3.12a. The more homogeneous rivet load distribution for a small radius R implies that the small barrel test may be quite appropriate for MSD observations. On the other hand fuselages with a large radius, and hence a less homogeneous load distribution, will not stimulate MSD. Another observation is based on the effect of the stiffness of the frames. Calculations for a less stiff connection between the frame and the skin (so called floating frames) will lead to a more homogeneous rivet load distribution along the lap joint, see the results in figure 3.12b-d. In figure 3.12b the displacements of the model are schematically presented. In the model the frame is given an initial displacement ΔR preceding pressurisation. The remaining boundary conditions make the frame infinitely stiff. Also the displacements in circumferential direction are prevented, which occurs to some extent in realistic configurations, especially with clips and castellations with a large shear stiffness. In figure 3.12b The rivet load transfer is presented for the end rows in the reduced-scale barrel. As can be deduced from figure 3.12c increases the load transfer for the edge rivets with relaxing the radial restraint of the frame. For all frame restraints four rivets have loads different from undisturbed. No provisions are required for the stiffness of the bulkhead in a reduced-scale barrel test set-up to increase the number of equally loaded rivets with this configuration. Even for radial displacements similar to the radial deflection of the skin the rivet load is reduced at the edges. The displacement of the overlap in circumferential direction with pressurisation still load the frame. This displacement in circumferential direction wants to occur due to the different radial displacements of the individual sheets of the overlap, as can be deduced from the model without bulkheads in figure 3.3. This displacement occurs to maintain equal strains and therefore membrane stresses in the individual sheets, despite the different radial displacements. With a frame present this deformation is resisted and loads the frame.

In figure 3.12d the load transfer in between the frames is presented for a radius of 2000 mm. With infinitely stiff frames the load transfer does not reaches its undisturbed magnitude with the frame pitch of 400 mm. The frame is transfers 31.5% of the hoop force. If the frame expands $^2/_3 \Delta R$ the load transfer becomes already more homogeneous. It then becomes more readily exposed to MSD conditions. Consequently the load transfer by the frame is reduced to 16% of the hoop force.

The rivet load distribution over the three rows, midway between the frames, is not affected by the radius of curvature. This is illustrated for a GLARE 3 3/2-0.3 cylinder in figure 3.13.

The distribution of secondary bending along the lap joint is not homogeneous in agreement with the inhomogeneous rivet load distribution. Secondary bending decreases near the stiff frames. That appears to a logical result in view of the deformation restraint at the frame. The inhomogeneous bending distribution is illustrated by figure 3.14 and the radial displacement results in figure 3.15. Figure 3.14 shows the bending around the longitudinal axis. The displacements in figure 3.15a are measurement results, while the results in figures 3.15b and c were obtained by FE calculations. In figure 3.15a the deformations of the skin and overlap in the reduced-scale barrel are obtained with LVDT measurements on elastically bent barrel specimen along the lap joint. The rotation of the overlap is prevented near the frame but rapidly becomes constant.

The finite element model is figure 3.15b is similar to figure 3.15a. As shown by figure 3.15b, a restraint on the radial displacements is observed close to the frames (1st rivet, 10 mm from the bulkhead). At 70 mm away from the rigid bulkhead the radial displacements and the overlap rotation are almost similar to the midbay results, as confirmed with the experimental results in figure 3.15a. Figure 3.15c shows the midbay results for a small cylinder radius (613 mm) and a large one (2820 mm, Airbus 340). Although the nominal radial displacements are highly different, the relative displacements and the overlap rotation are practically similar. As a consequence, secondary bending at the midbay position will also be the same.

3.4　Strain gauge measurements

Strain gauge measurements have been performed on 2024-T3 and GLARE 3 reduced-scale barrel specimens and on GLARE 3 lap joints in a full-scale Airbus A340 barrel at the Deutsche Airbus facility in Hamburg. The purpose was to compare stress distributions and secondary bending results. It should indicate the relevance of fatigue tests carried out in the reduced-scale barrel.

(a) Measurements on 2024-T3 cylinders

Strain gauges are bonded on the faying surface of a barrel specimen at locations close to the rivets of the critical rivet rows, i.e. the top row and the bottom row, see figure 3.16.

Hoop stress results of an elastically bent cylinder are presented in figure 3.17. The applied hoop stress is also indicated in this figure. It is in close agreement with a strain gauge measurement away from the lap joints and the pressure bulkheads. The midbay stress results are still somewhat below the hoop stress, but it should be recalled that the strain measurements were made in a locally non-homogeneous stress field. The stress results agree with the non-homogeneous rivet load distribution along the lap joint. There are small differences between the results for the top row and the bottom row. This might be due to slightly different situations around the rivets of the two end rows as a result of non-symmetric plastic deformations in the outer and the inner sheet.

Results of the secondary bending stresses are presented in figure 3.18 for two 2024-T3 cylindrical specimens, one specimen with elastically bent sheets and a second one with roll-formed sheets (in the latter case 3 results only). There is a significant difference between the results of the two cylinders. In a third test series an elastically bent part of the first cylinder was also tested uniaxially as a flat specimen in a servo-hydraulic 1000 kN test machine. These results differ considerably from the results of the same strain gauges in the barrel test set-up. However, they reasonably agree with the results of the cylinder with the roll-formed sheets tested in the reduced-scale barrel test set-up.

The bottom row results of the elastically bent sheet cylinder agree with the FE calculations. At the pressure bulkhead, lap joint rotation is prevented, which leads to reduced secondary bending. However, secondary bending at the top row is relatively small along the entire lap joint, and bending even occurs in the opposite direction to be expected from the eccentricity. It is thought that this result should be associated with imperfections in the joint in combination with using elastically bent sheets for the cylinder production. This is partly confirmed by the results of the same lap joint loaded as a flat specimen. The secondary bending stresses now have the same sign, although a difference between the top row and the bottom row remains. The bending in the barrel specimen is more severe compared to the bending in the flat specimen. It indicates that the present imperfections are more severe in pressurised fuselage specimens. The intention has been to avoid this situation in the test on the GLARE 3 barrel specimen by using roll-formed sheets and preventing imperfections by flush riveting installation.

(b) Measurements on GLARE 3 3/2-0.3 barrels

Stress measurements on GLARE 3 lap joints were carried out on:
- A barrel specimen with roll formed sheets.
- The GLARE 3 3/2 0.3 crown section of the Airbus A340 full-scale barrel (diameter 5.640 m, length 4770 m).
- An uniaxially loaded flat specimen.

Figures 3.19a and 3.19b show the results of stress measurements for the top row and the bottom row respectively. The results have been plotted as a function of the internal

pressure. The strain gauges were again located close to the rivets, in the centre of the flat specimen, and at a midbay position for the barrels. Figure 3.19 also gives the theoretical stress in the aluminium layers corresponding to the nominal hoop stress $\Delta pR/t$. This stress is larger than the hoop stress because of the smaller elastic modulus of the fibre layers.
In figure 3.19, the stress measured in the reduced-scale barrel test is similar to the stress measured on the flat specimen. This agrees with the calculations of the previous section. The measurements also confirm that there is practically no restraint on the radial displacement in the reduced-scale barrel test midway between the bulkheads.
For the full scale barrel the radial expansion is larger. As a consequence, the radial restraint on the radial expansion will become significant as discussed before. Moreover, the longitudinal stiffeners further contribute to the radial restraint. As shown by the results in figure 3.19. it leads to a reduction of the stress level by a factor of about 1.2. The same trend is observed for the top row and the bottom row. The reduced stress level is favourable for fatigue of the lap joint.

The bending stress is plotted in figure 3.20 as a function of the applied pressure Δp. The secondary bending stress in the reduced-scale barrel test and on the flat uniaxially loaded lap joint are practically similar for the bottom row (figure 3.20b) and approximately similar for the top row (figure 3.20a). However, these bending stresses for the top row and for the bottom row are different. The strain gauges near the rivets of the top row and the bottom row are applied at anti-symmetric locations. However, the stress fields close to the rivets are not anti-symmetric for the two rows, because the countersunk rivets are not in an anti-symmetric configuration. Different results for the top row and the bottom row are then possible.

The secondary bending stresses measured on the full-scale A330 barrel are significantly smaller than in the reduced-scale barrel test, see figure 3.20. The effect of the lower hoop stress in the full-scale barrel can be eliminated by plotting the bending stress as a function of the measured circumferential stresses. This has been done in figure 3.21. For the top row the results of the reduced-scale barrel and the full scale barrel then appears to be similar, but the large reduction of the bending stress at the bottom row remains. In the Airbus fuselage longitudinal stiffeners are located at a pitch of 16 to 18 cm. A stiffener is also connected to the bottom row, see figure 3.22. The stiffeners are also connected to the frames. The stiffener will thus reduce the lateral expansion at the bottom row, but it leaves the lap joint free to rotate. As a result, the bottom row becomes less critical, and it does not increases the bending severity at the top row, as confirmed by the results in figure 3.21.

4   FATIGUE TEST RESULTS

4.1   Crack initiation and growth

The effect of biaxiality and pressurisation on crack growth is investigated by comparing the test results of the reduced-scale barrels with the uniaxially loaded flat specimens. Figure 4.1 shows the results for 2024-T3. Crack growth in the reduced-scale barrel test is considerably faster than in the flat specimen. The average crack growth rate is approximately 5 times larger for the barrel specimen. Bulging of the fatigue crack has increased the growth rate. Due to the small radius of curvature, a large internal pressure was necessary to achieve the required membrane stress. This high internal pressure (Δp is 1.583 bar for σ_{hoop} equal to 97 MPa) increases the bulge factor considerably [ref. 4].

Similar comparative tests were performed on GLARE 3 3/2-0.3 specimens. The results in figure 4.2 show crack growth starting from a centre crack of 20 mm. A linear crack growth is found, also in the barrel under the pressurisation cycle. In the barrel test, the maximum pressure Δp is equal to 2.83 bar to obtain the hoop stress of 124 MPa. The crack growth rate in the reduced-scale barrel test is 1.7 times larger than the growth rate in the flat centre cracked specimen. Crack growth of a smaller crack was observed in another couple of comparative tests. Crack growth now started from a 4 mm blunt notch hole. As shown by the results in figure 4.3, the difference in crack growth rates for the flat sheet and the barrel specimen becomes smaller. Crack edge bulging is considerably reduced due to the intact crack bridging fibres. The fibres were cut by the initial notch over 4 mm only.

4.2   Curved panel test results

The test results for these specimens show many collinear cracks, which indicates a homogeneous stress distribution along the rivet lap joint. Later in the test, severe multiple site damage with high crack growth rates has been found to occur.

The fatigue lives of the two 2024-T3 lap joint specimens were 142 kc and 176 kc respectively. Small crack nuclei of 2 mm were present after 124 kc and 161 kc respectively. Two flat specimens of the same configuration, dimensions, and rivet squeeze force were tested at the same stress level. The fatigue lives were are 549 kc (initiation 460 kc) and 575 kc (initiation 434 kc), see figure 4.4. The crack free life is approximately 3.5 times smaller in the curved set-up, and the crack growth afterwards about 5 times faster. Elastic bending increases the severity of the bottom row and bulging of cracks can contribute to higher crack growth rates.

The fatigue life of the GLARE 3 3/2-0.3 specimen is 551 kc at 124 MPa (see figure 4.4). Flat specimens (width of 140 mm) with a similar lap joint configuration failed at 504 kc. The elastic curvature of the sheets affects the bending stress mostly at the outer layer. It

leads to earlier crack initiation for both monolithic and laminated materials. However, GLARE joints give similar fatigue results, because of the laminated character and the absence of significant crack bulging due to intact fibres.

4.3 Reduced-scale barrel test results

2024-T3 specimens
If the sheets of a specimen for a reduced-scale barrel test are elastically bent, the maximum bending stresses induced are theoretically 60 to 70 MPa. A matter of concern is that the overlap with its larger bending stiffness will remain approximately flat during the bending operation, see figure 4.5. That may introduce more secondary bending.

In the first 2024-T3 barrel specimens, two of the three lap joints were squeezed with 14 kN and the 3rd one with a lower squeeze force of 12 kN. The fatigue life of the latter joint was about 20% lower than the fatigue lives of the other two lap joints, see figure 4.6. After failure of the 12 kN squeezed lap joint, it was repaired for continuing the barrel test with the other two lap joints. The lower squeeze force has led to slightly smaller driven heads, i.e. 0.4 mm smaller than for the 14 kN squeezed rivets. Apparently, the barrel test confirms the significance of the squeeze force for the fatigue life under biaxial loading.

The second 2024-T3 barrel specimen was made from roll-formed sheets. The fatigue life was increased from an average value of 107 kc for the elastically bent barrel specimen to 189 kc, which is about 80% more life. Apparently, the better cylindrical shape is favourable, also because the imperfections will be smaller. The barrel test results are compared to the results of the uniaxially loaded specimens, see figure 4.6. A summary of the crack initiation lives is given below:

Preparation	Test set-up	R (mm)	Fatigue load	Av. crack initiation life [kc]
elastically bent	barrel	613	biaxial	108
elastically bent	curved	2000	uniaxial	159
roll formed	barrel	613	biaxial	157
flat	tensile machine	∞	uniaxial	562

It confirms that elastically curved sheets should be avoided, although fuselages with larger radii are in a better position. Roll forming gives an improvement, but at the same time it must be realised that imperfections, due to non-flush rivet installation and careless production processes can be harmful for the fatigue life in view of the introduction of imperfections. For the tested 2024-T3 configurations imperfections were present due to the non-flush rivet installation and large ratio of D_0/t. They were more severe for the

elastically bent sheet compared to the rolled sheet, as confirmed by bending measurements in figure 3.18.

In the above considerations, it was tacitly assumed that biaxial loading and uniaxial loading will give similar fatigue life and crack growth results. It is difficult to give a really good proof of this conclusion. However, as shown before, the secondary bending in riveted lap joints is not really affected by biaxial loading. Further, K_t-values of cracks are insensitive to transverse load. It appears that a negligible effect of the biaxiality could be a pragmatic approach.

GLARE 3 3/2-0.3 specimens

The roll formed GLARE 3 barrel was riveted with flush installed rivets to avoid imperfections during riveting. The fatigue life was above 370 kc for both specimens, when it was decided to stop the test. It is noteworthy that the roll formed barrel specimen with 18 complete ligament failures was still able to bear the fatigue load during 40 kc (see figure 4.7).

The life of the two lap joints with the rivet diameter D_0 equal to 4.0 mm is shorter than the fatigue life of the uniaxially loaded flat specimen (504 kc), see figure 4.6. The uniaxially loaded GLARE 3 specimen (same configuration), loaded in the elastically bent condition (R = 2000 mm), is outperforming this (551 kc).

The third lap joint of the GLARE 3 barrel specimen (D_0 is 4.8 mm) has also been tested up to 370 kc, which is more than nine times design life. The crack growth development in the 1st, 2nd and 3rd layer are presented in figures 4.8a and 4.8b for the top row and the bottom row respectively. The fatigue damage at that moment covered 63.1% of the net section at the top row, and 62.1% at the bottom row. As shown, the crack growth occurs in a similarly moderate way as already observed in chapter 12, in contrast to the behaviour of 2024-T3. Figures 4.8c and 4.8d show some intermediate stages of fatigue damage. They do give the impression of MSD, but actually it does not lead to accelerated crack growth.

A flat specimen with a similar lap joint configuration and rivet installation conditions has been tested at the same hoop stress level. The fatigue life was 768 kc, significantly higher than in the barrel test. The fatigue damage at 370 kc was 27% at the top row, significantly less than in the barrel test. A comparison of the crack initiation lives of the flat specimen and the barrel specimen is made in figure 4.9. It illustrates that the reduced-scale barrel test implies a more severe loading condition than the uniaxially tested flat specimen.

After stopping the fatigue test on the roll-formed GLARE 3 barrel, a residual strength test has been performed by increasing the internal pressure. Static failure occurred in the top row with the larger fatigue damage being present. It occurred at a nominal hoop stress of 257 MPa. This result is plotted in figure 4.10a with some results of uniaxially loaded flat specimens (data from [ref. 3]). Although the cracks in the barrel specimen were not homogeneously distributed along the width, the residual strength does agree very well with the results of the flat specimen. The specimen after failure is shown in figure 4.10b.

4.4   Evaluation

The results of the GLARE 3 barrel test are assumed to be conservative for riveted GLARE lap joints in a fuselage of a large aircraft. This is primarily due to the relatively small diameter of the reduced-scale barrel.

The fatigue damage development, as observed in the reduced-scale barrel test, is presented in figure 4.11. The results apply to the Airbus 340 full-scale barrel configuration. Assuming an operational life of twenty years with 2,000 flights in a year, a period of 40,000 cycles corresponds to one design life. The test then indicates that the residual strength is reduced to 257 MPa after about nine times design life. This result applies to a nominal hoop stress level of 124 MPa. In other words the residual strength is still more than twice the nominal hoop stress. It thus easily satisfies the slow crack growth option of the present airworthiness requirements. In addition, there is ample time to detect fatigue damage by eddy current inspections, while very long inspection periods are acceptable. In other words, also under the damage tolerance requirements, the results as presented in figure 4.11 allow relatively long inspection periods.

A comparison between 2024-T3 and GLARE 3-3/2-0.3 based on the barrel tests can not easily be made. The configuration for the 2024-T3 barrel specimens was actually more representative for a much smaller aircraft. However, the following data of the reduced-scale barrel tests on roll-formed specimens are illustrative:

material	specific mass [g/cm³]	hoop stress [MPa]	fatigue life [kc]	crack growth rate
2024-T3	2.78	97	189	relatively high
GLARE 3 3/2-0.3	2.52	124	370	low

5   CONCLUSIONS

Fatigue tests at nearly zero stress ratio and strain gauge measurements have been carried out on riveted lap joints. The investigation included (i) uniaxially loaded flat specimens, (ii) elastically bent specimens (radius of 2000 mm), uniaxially loaded by internal pressure, (iii) biaxially loaded cylindrical specimens in a reduced-scale barrel test set-up (radius of 613 mm), and (iv) a full-scale barrel set-up test (radius of 2820 mm) for the Airbus A340. The materials investigated were 2024-T3 and GLARE 3 3/2-0.3. During the fatigue tests crack growth records were made. The results of this study are summarised below.

- The hoop stress and the secondary bending of a riveted joint vary between the frames of a fuselage with a maximum midway between the frames. This maximum is more pronounced for large fuselages and stiff frames with a stiff frame/skin connection. For a small fuselage and for a low stiffness frame and frame/skin connection, the major part of the riveted lap joint is subjected to an almost uniform hoop stress and secondary bending. This condition stimulates the occurrence of multiple-site damage. It implies that fuselages with so-called floating frames, if fatigue cracks are imminent, are more likely to see multiple-site damage.

- The inhomogeneity of the secondary bending along a riveted lap joint between the frames corresponds with a similar inhomogeneity of the distribution of the rivet loads in the critical end rows (top and bottom row).

- The secondary bending and the lap joint overlap rotation at the midbay location are practically independent of the fuselage radius and the biaxiality ratio. They are similar to secondary bending and lap joint overlap rotation observed in flat uniaxially loaded riveted lap joints specimens.

- The above conclusions are supported by FE calculations, strain gauge measurements and measurement of the radial displacements of the sheets. Further support is coming from crack nucleation sites observed in fatigue tests.

- Fatigue tests on a 2024-T3 reduced-scale barrel specimen confirmed that a lower squeeze force leads to a shorter life.

- Flat uniaxially loaded specimens generally provide longer fatigue lives than pressurised barrel specimens for both materials. Also a larger radius give better results. The reduced-scale barrel test will give conservative information on fatigue crack initiation lives and crack growth.

- Elastically bent sheets on a pressurised cylinder lead to shorter lives than roll formed sheets. This is especially important for the reduced-scale barrel test with its relatively

small radius. Roll formed sheets lead to lower secondary bending and significantly longer fatigue lives. It is important that the sheet edges, which will be part of the overlap, are roll formed, instead of being flat.

- In the full-scale Airbus barrel the circumferential stress and the secondary bending stress at the midbay location were lower than in the reduced-scale barrel specimens when loaded to the same nominal hoop stress. This is due to more restraint on radial skin displacements by the frames and the longitudinal stiffeners riveted together with the bottom row of the lap joint. The secondary bending of a real fuselage structure can not easily be simulated in a simple specimen test in view of different restraints on radial displacements. The displacements have a large effect on secondary bending and thus on fatigue.

- Flat uniaxially loaded specimens generally provide longer fatigue lives than pressurised cylindrical specimens. The discrepancy is recognised by the aircraft industry when considering results of relatively small riveted lap joint specimens and the fatigue life of the real fuselage structure. The discrepancy is partly associated with the influence of the built-in stresses, stiffening elements, while the most important part should be related to squeeze force effects, possible imperfections of the riveted joints in the structure as a result of the manufacturing process, and to workmanship in general. Such aspects can not easily be quantified. However, it appears that worthwhile life improvements can be achieved by more careful process control requirements. Force controlled squeezing is recommended in this respect. Hand riveting can easily lead to undesirable imperfections.

- The fatigue behaviour of riveted 2024-T3 and GLARE 3 3/2-0.3 lap joints under biaxial loading is completely different. For the 2024-T3 reduced-scale barrel specimens the crack growth period is relatively short with rapidly increasing crack growth rate. In the GLARE 3 barrel specimens, crack growth occurred very slowly without a noticeably increasing growth rate. With the eddy current technique it was easy to detect small cracks and to follow crack growth in the first aluminium layer at the mating surface. In a test at a hoop stress of 124 MPa crack growth was followed until 370 000 cycles. The residual strength at that moment was found to be 257 MPa in the skin material, which is above ultimate design load.

REFERENCES

[1] Brite Euram BE2040, "Fibre reinforced metal laminates and CFRP fuselage concepts", Technical Annex, August 1994.

[2] Holleman, E, Fatigue strength of riveted lap joints in GLARE 3 3/2-0.3 reduced-scale barrel, curved panel and flat panel design - Program definition (BE2040 subtask 4.1), Document B2-95-03, Structures and Materials Laboratory, Faculty of Aerospace Engineering, Delft Univ. of Techn., Delft, April 1995.

[3] Müller, R.P.G., An experimental and analytical investigation on the fatigue behaviour of fuselage riveted lap joints, PhD thesis, Faculty of Aerospace Engineering, Delft Univ. of Techn., Delft, ISBN 90-9008777, October 1995.

[4] Chen, D, Bulging of fatigue cracks in a pressurized aircraft fuselage, PhD thesis, Faculty of Aerospace Engineering, Delft Univ. of Techn., Delft, January 1991.

[5] Borsboom, C, Eddy current testing of Fiber Metal Laminates, Structural Laminates Company, Technical report TD-R-93008, Delft The Netherlands, June 1993.

[6] Timoshenko, S.P., and S. Woinowsky-Krieger, Theory of plates and shells, second edition, ISBN 0-07-085820-9, McGraw-Hill international editions (and Ae102c).1

[7] Ernst, Stijfheid en Sterkte 4, Lecture bw71, Faculty of Mechanical Engineering and Marine Technologies, Delft University of Technology.

[8] ABAQUS 5.2 reference manual.

LEFT BLANK INTENTIONALLY
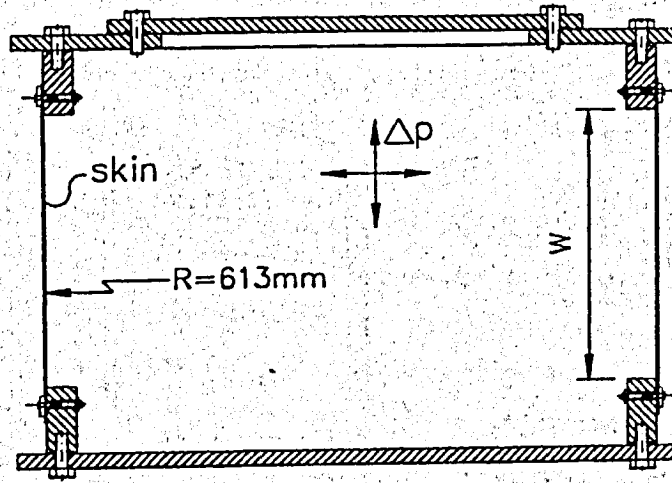
Figure 2.1 *Schematic illustration of the reduced-scale barrel test set-up [ref. 3].*
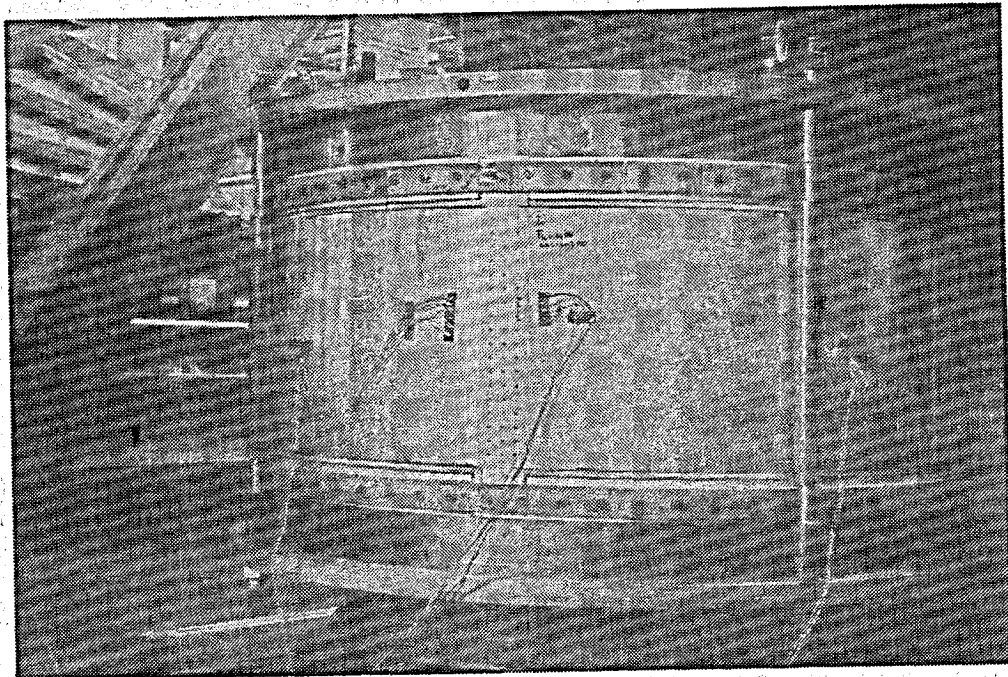
Figure 2.2 *Photograph of reduced-scale barrel test set-up [ref. 3].*
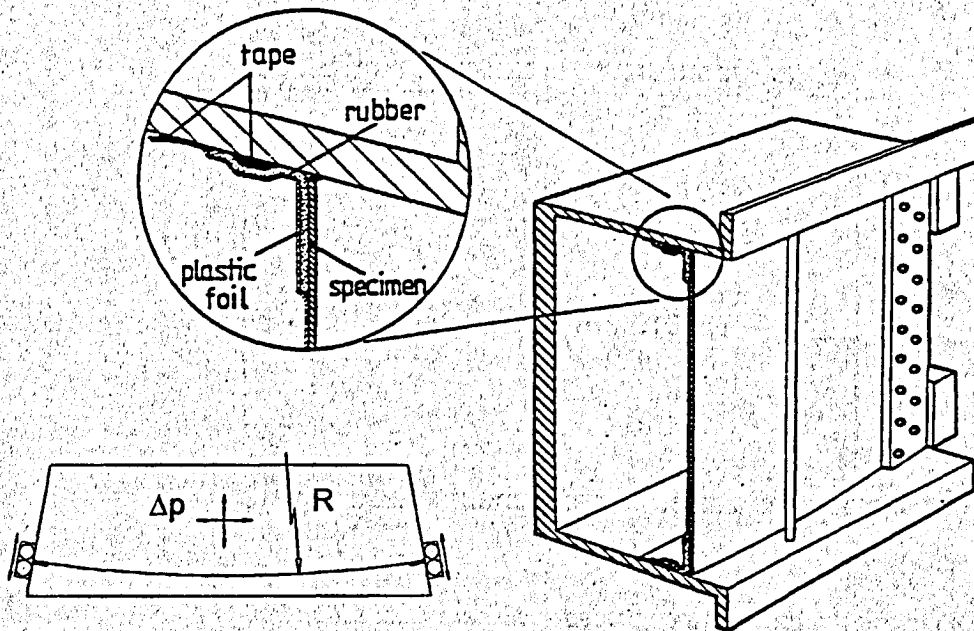
Figure 2.3 *Schematic illustration of the curved panel test set-up (R = 2000 mm) [ref. 4].*
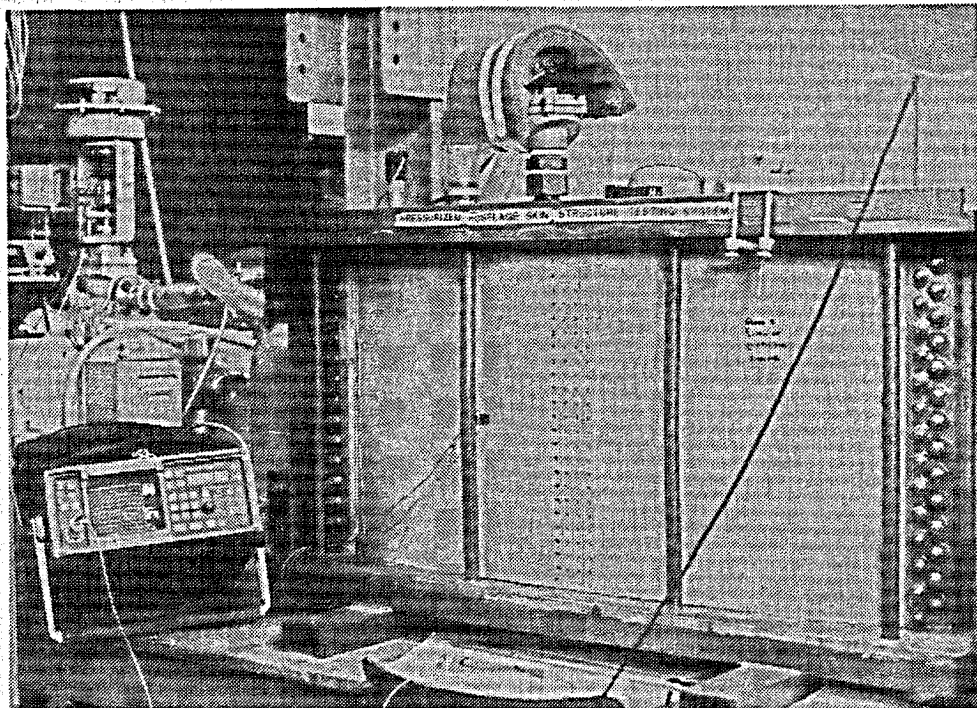
Figure 2.4 *Photograph of curved panel test set-up [ref. 3].*

configuration:
3-row riveted joint
s=p=20mm
rivet:NAS1097AD5-5
rivet squeeze force:14kN

strain gauges

lateral gauges

450

840

20

500
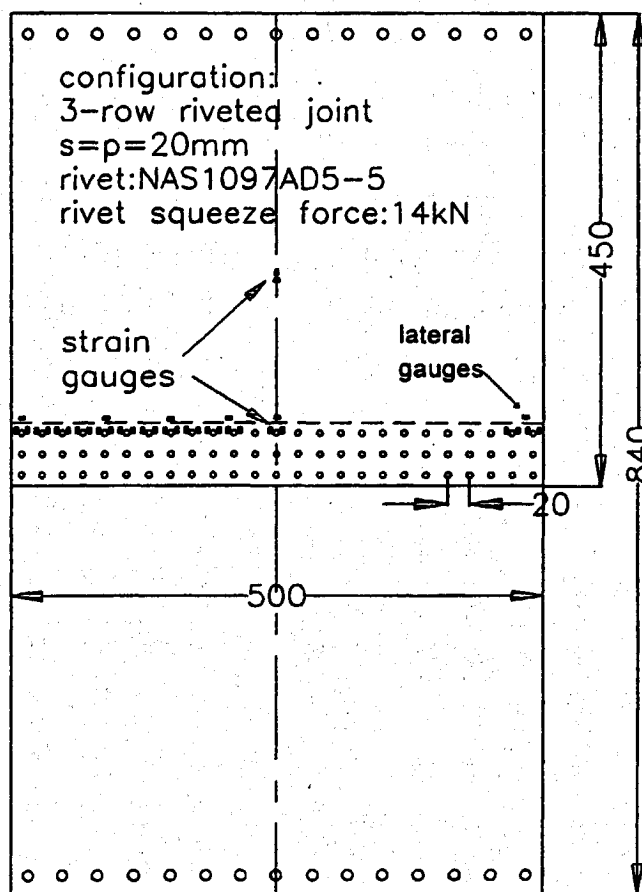
Figure 2.5 *Schematic illustration of the flat panel geometry.*

Steel blocks

clamping pressure

free edge
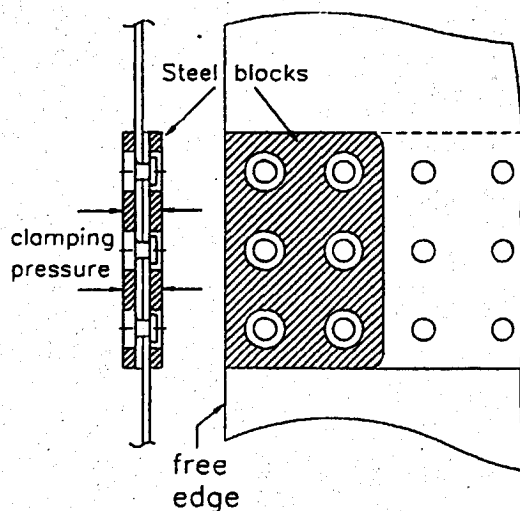
Figure 2.6 *Steel blocks attached to the flat specimen edges to reduce local secondary bending [ref. 3].*

Figure 2.7

Memorandum M-721

Figure 2.7 caption within figure:

Glare 3-3/2-0.3

☐ Al2024-T3,t=0.3mm

▨ prepreg,t=0.125mm

☐ = Aluminum Layer

■ = Prepreg Layer

■ = Fatigue Critical Location

Layer 3
Layer 2
Layer 1 } Top Sheet
Layer 1
Layer 2 } Bottom Sheet
Layer 3

rolling direction
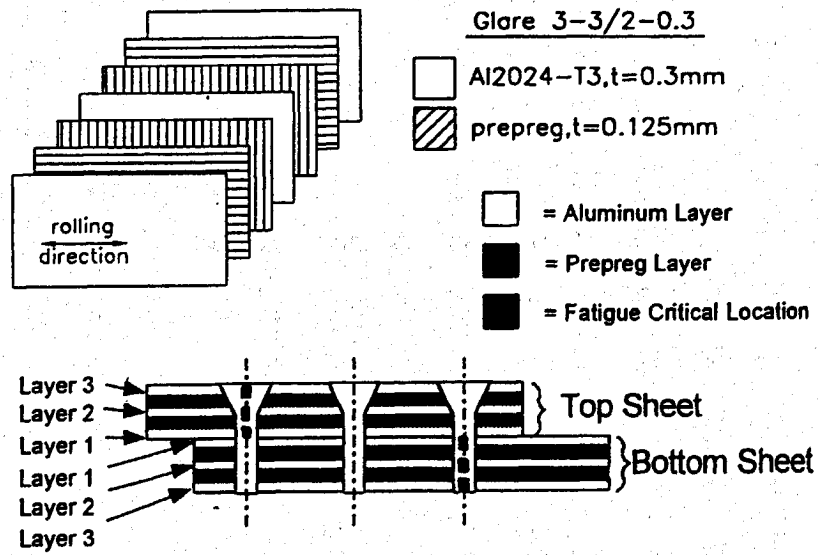
Figure 2.7 *Numbering of aluminium layers for GLARE 3 3/2-0.3.*
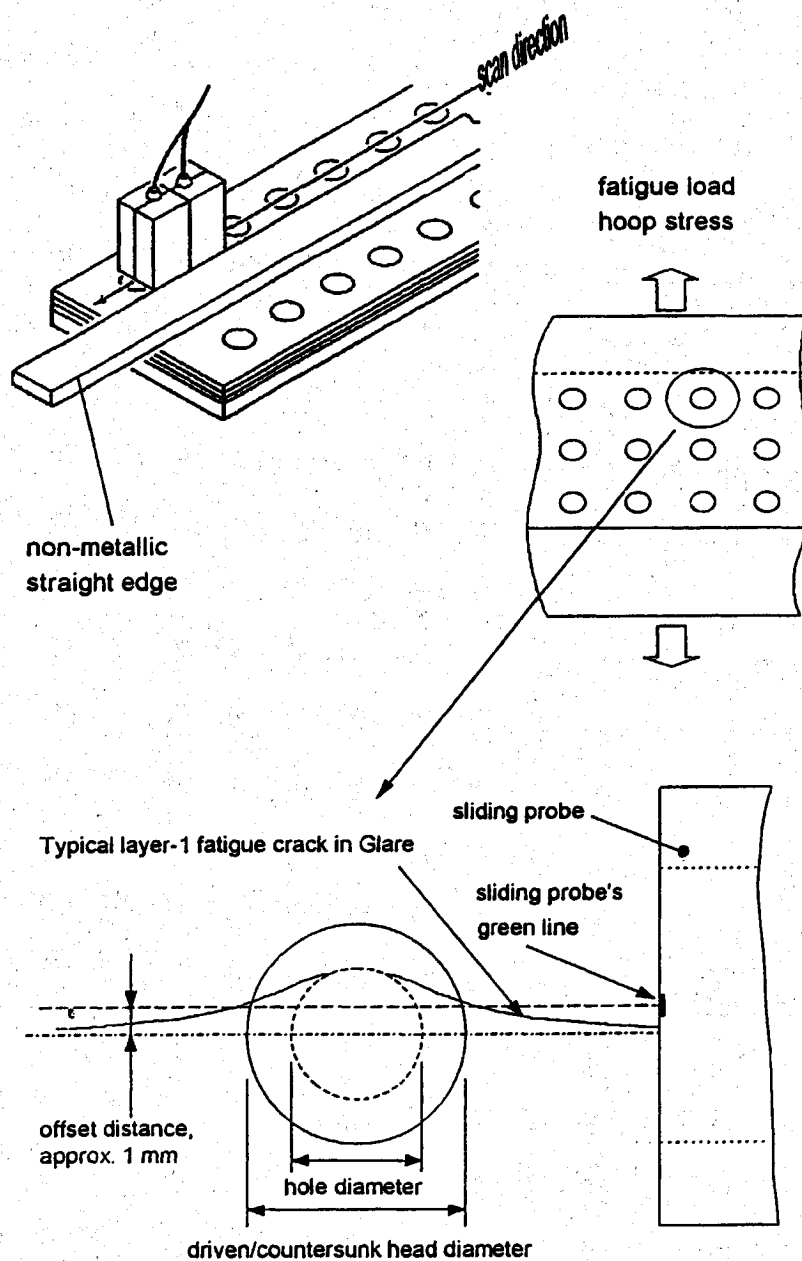
Figure 2.8 *Sliding probe of Nortec eddyscope and proposed scanning path location for crack detection in mating layers in a riveted lap joint [ref. 3].*
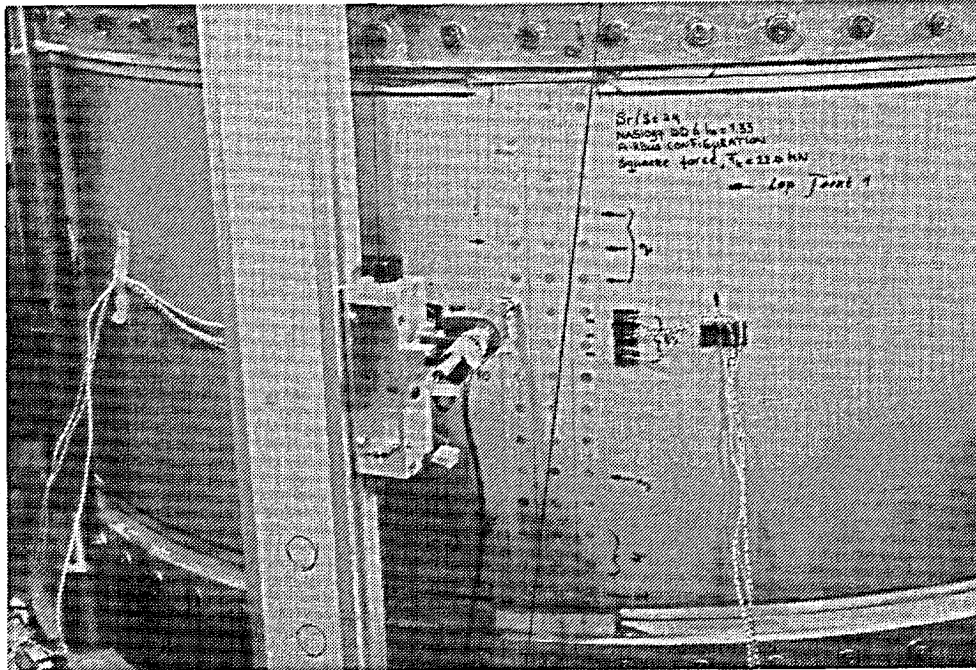
Figure 2.9   *Reduced-scale barrel with LVDT displacement measurement equipment and strain gauges [ref. 3].*

c   height of cylindrical part
h   countersink depth
t   sheet thickness
d   rivet diameter

Knife-edge condition: c ≤ 0 mm
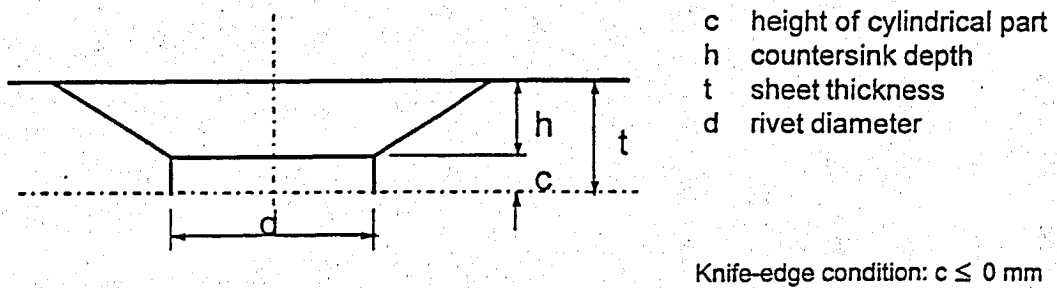
Figure 2.10 *Definition of knife-edge.*

type I, critical countersunk sheets

type I, critical non—countersunk sheets
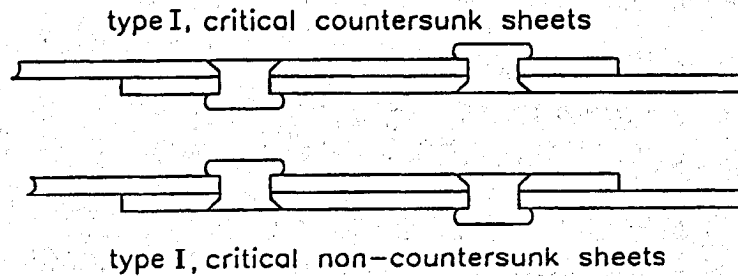
Figure 2.11 *Anti-symmetric two-row riveted lap joint coupons.*

type I ▼ ▽

type II ● ○

3250   >3250

Alclad2024,t=1 mm
2-row riveted joint
s=20mm,p=40mm
$\sigma_{applied}$= 97,R=0.05,
W=60 mm
NAS1097AD5,D$_o$=4mm

δ=0.0mm

δ=0.1mm

cycles to failure [kc]

900
800
700
600
500
400
300
200
100
0

0   5   10   15   20   25

squeeze force [kN]

1   1.05   1.16   1.3   1.42   1.58   1.7

D/D$_0$
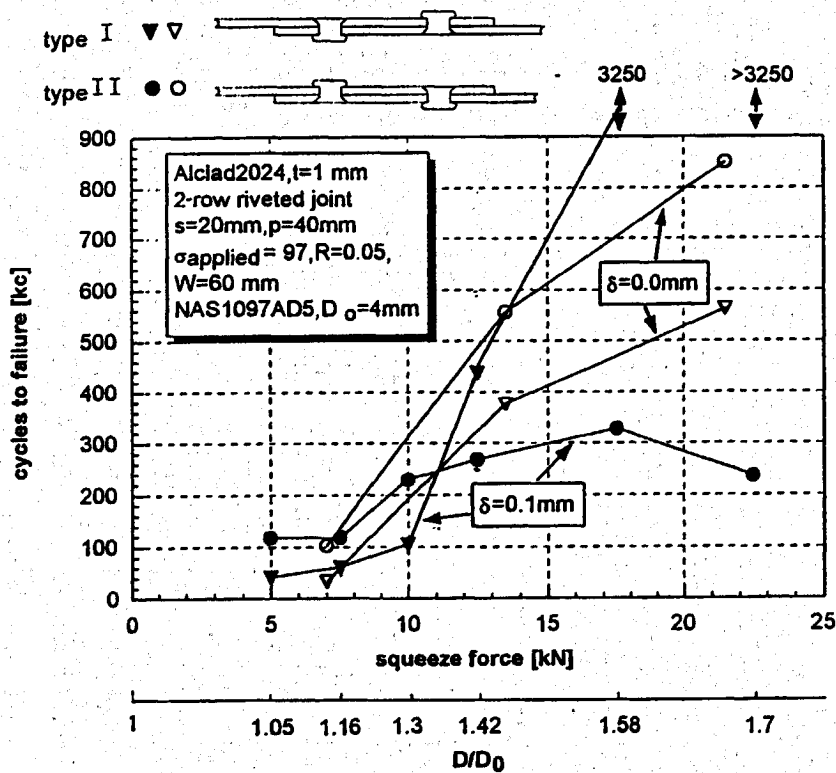
Figure 2.12 *Fatigue performance of lap joints with critical countersunk holes or with critical non-countersunk holes. Comparison between specimens with smooth surface (δ = 0 mm) and specimens with imperfections (δ = 0.1 mm) [ref. 3].*
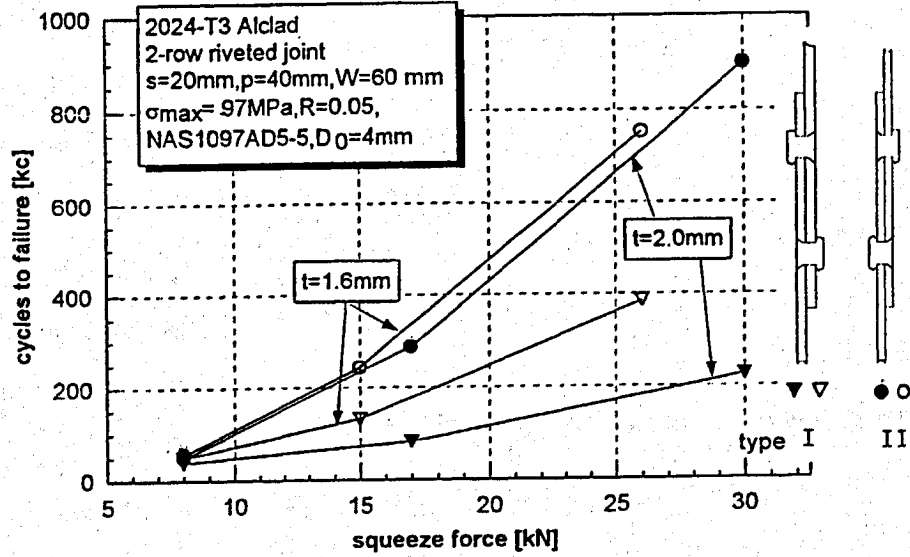
Figure 2.13 *Fatigue test results for anti-symmetric two-row lap joint coupons. Effect of the squeeze force and the sheet thickness [ref. 3].*
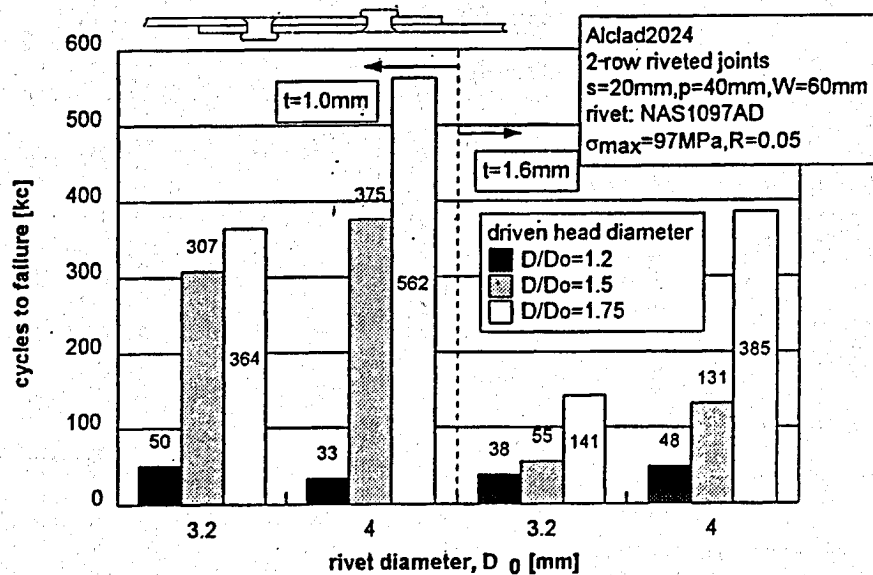
Figure 2.14 *Comparison of fatigue performance to demonstrate the effect of the squeeze force [ref. 3].*
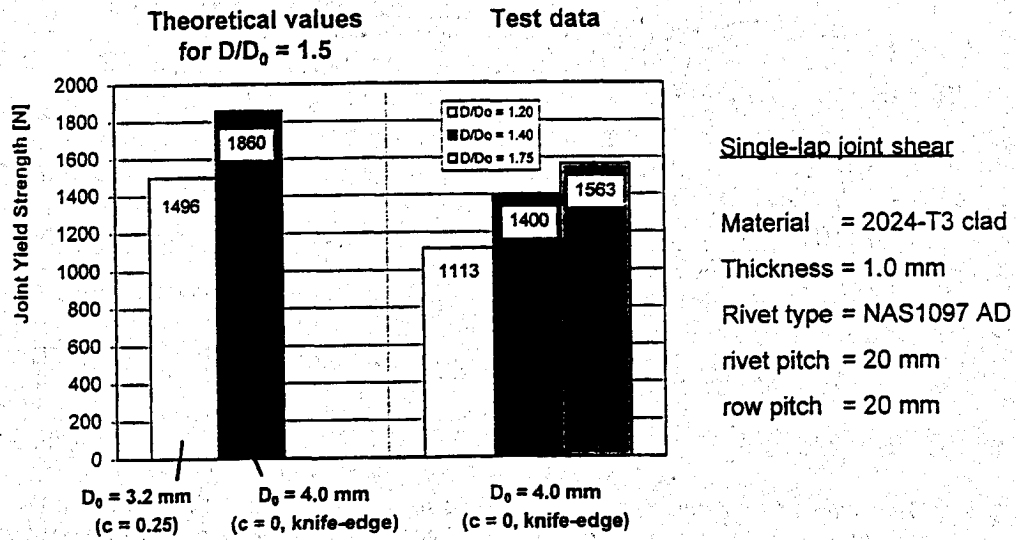
Figure 2.15 *Comparison of joint ultimate strength to demonstrate the effect of the squeeze force.*

Figure 3.1 diagram labels: 20, 10, t=0.6mm, t=1.0mm, Δp (inside) skin, bulkhead

Glare3-3/2-0.3,t=1.4mm
radius of curvature=613mm
ΔP=0.283MPa,σ_{hoop}=124MPa (χ=0.5)

Chart axis labels: radial displacement [mm]; axial coordinates [mm]; FE calc.; calculated without bonded doublers (analytical); measured in small scale barrel with bonded doublers; Bulkhead; Bulkhead
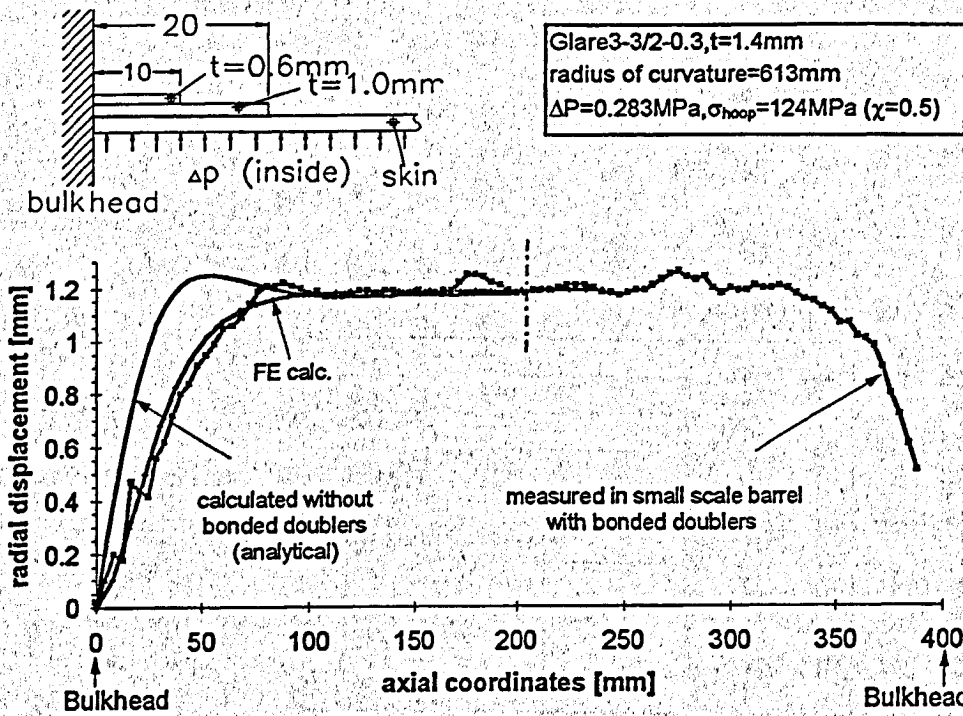
Figure 3.1 *Calculated and measured radial skin displacements according to (i) an analytical calculation (without end-doublers), (ii) FE- calculations (with end-doublers) away from the lap joint, and (iii) measurements away from the lap joint in the reduced-scale barrel test (W = 420 mm) [ref. 3].*

Labels: stiffener, frame
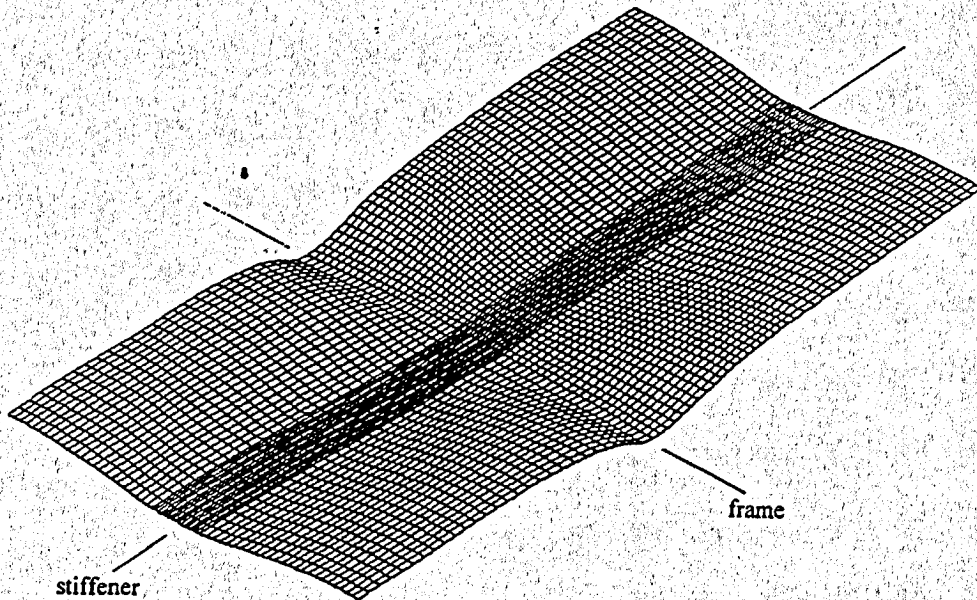
Figure 3.2 *Pillowing of pressurized fuselage in FE mesh [ref. 3].*

middle row

2024-T3, t=1.0mm, E=73000MPa, v=0.305
3-row riveted lap joint
s=p=20mm
radius of cylinder:1500mm
Δp=0.0647MPa,σhoop=97MPa
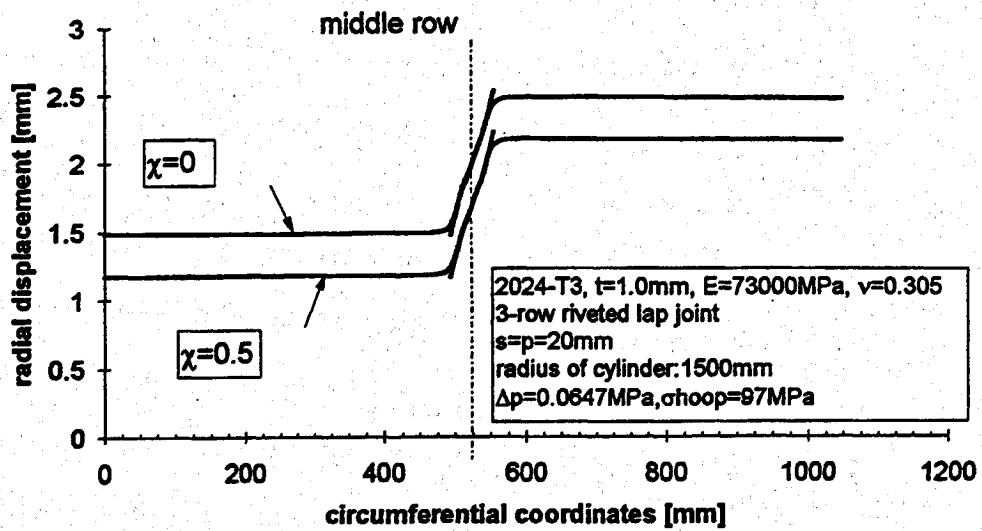
Figure 3.3 *Radial displacements of the neutral lines in a riveted lap joint in an unstiffened cylinder under biaxial loading (χ = 0.5) or without biaxial loading (χ = 0) calculated by use of a 2d finite element model [ref. 3].*

Figure 3.4

Memorandum M-721
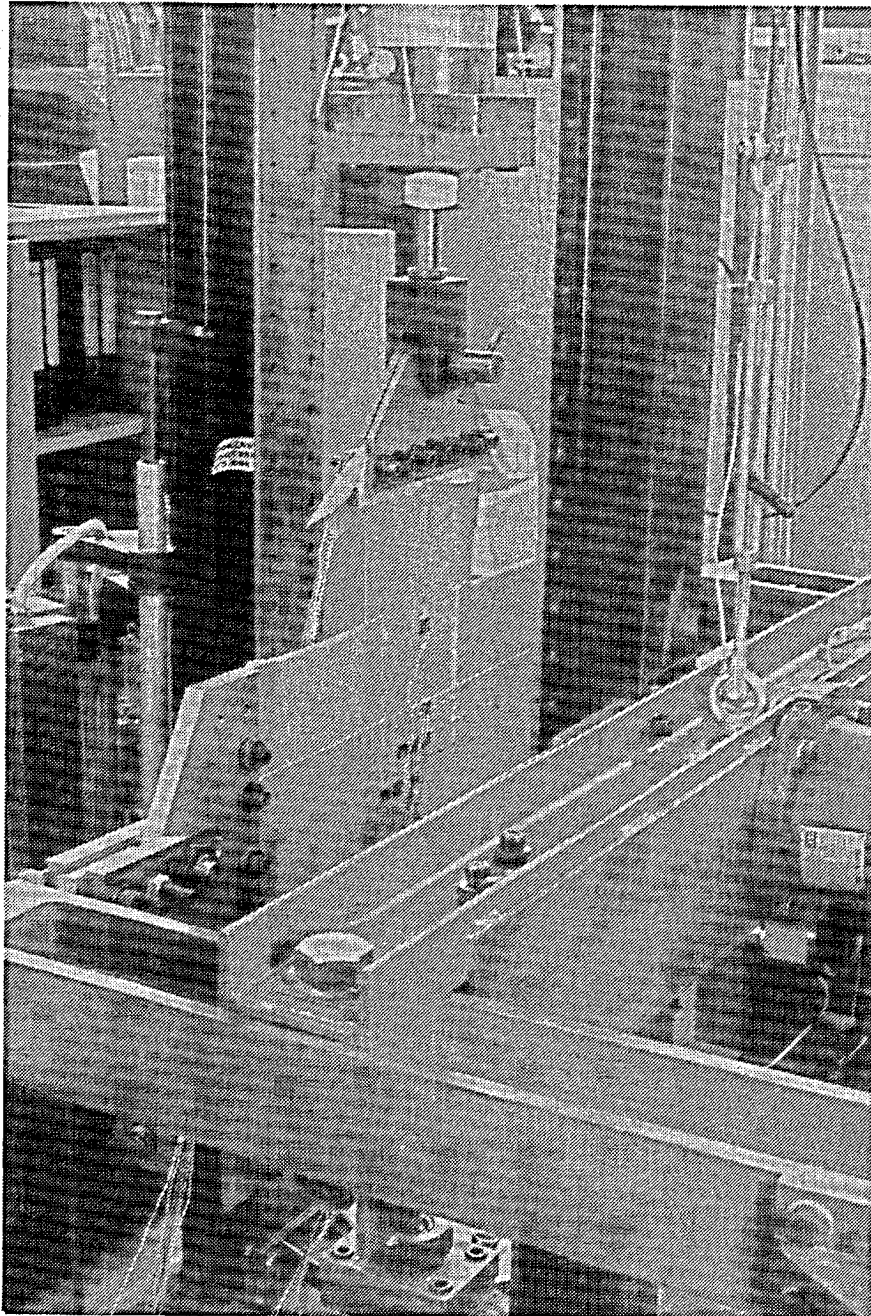
Figure 3.4 *Set-up for biaxial testing of riveted lap joint coupons. Specimen width is 220 mm [ref. 3].*
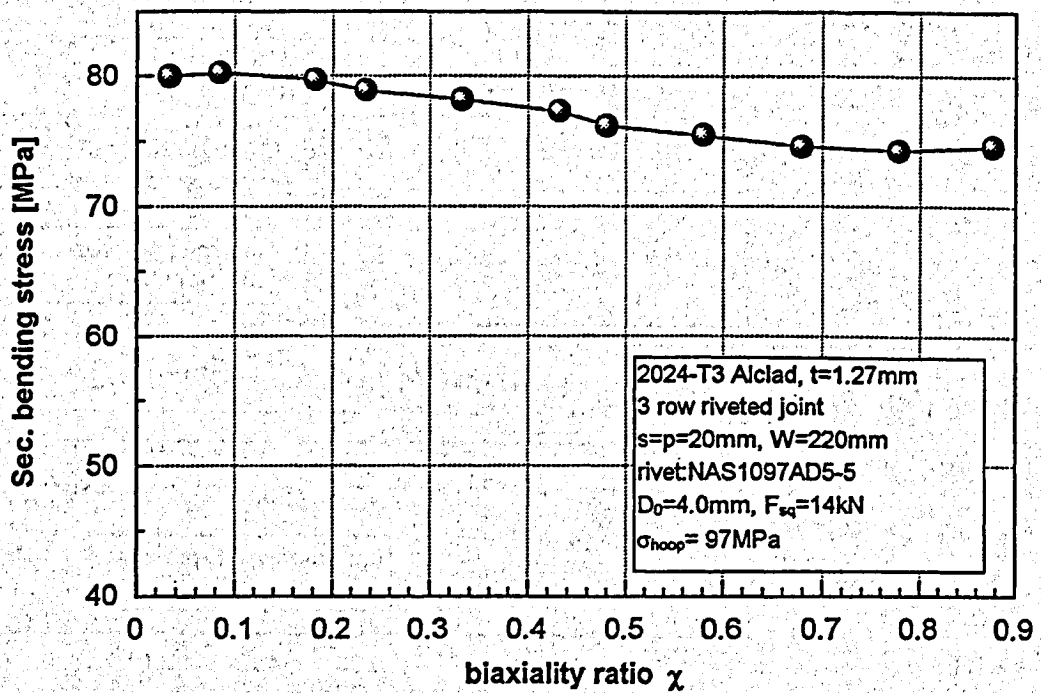
Figure 3.5 *Secondary bending measurements with strain gauges at the centre of the riveted joint specimen at the bottom row in the flat biaxial test set-up as a function of the biaxiality ratio.[ref. 3].*
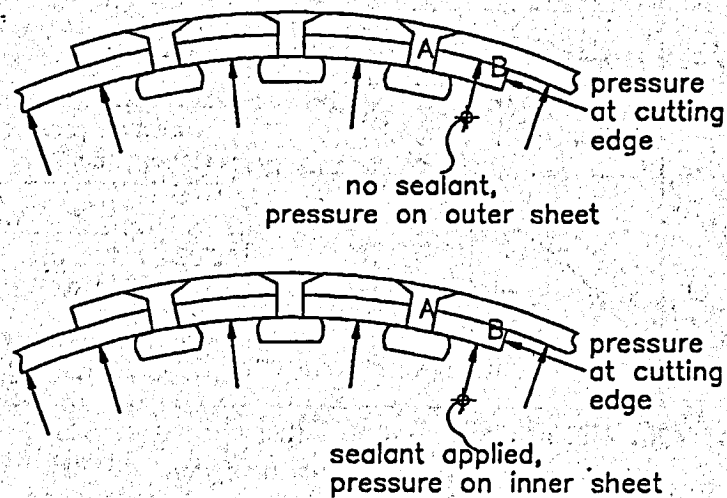
Figure 3.6 *Finite element modelling options. Pressure on free edge (AB) of the inner sheet (interfaying sealant used) or pressure on the outer sheet of this part (no interfaying sealant) [ref. 3].*

Figure 3.7   Memorandum M-721

(a) Load transmission by the critical end rows.
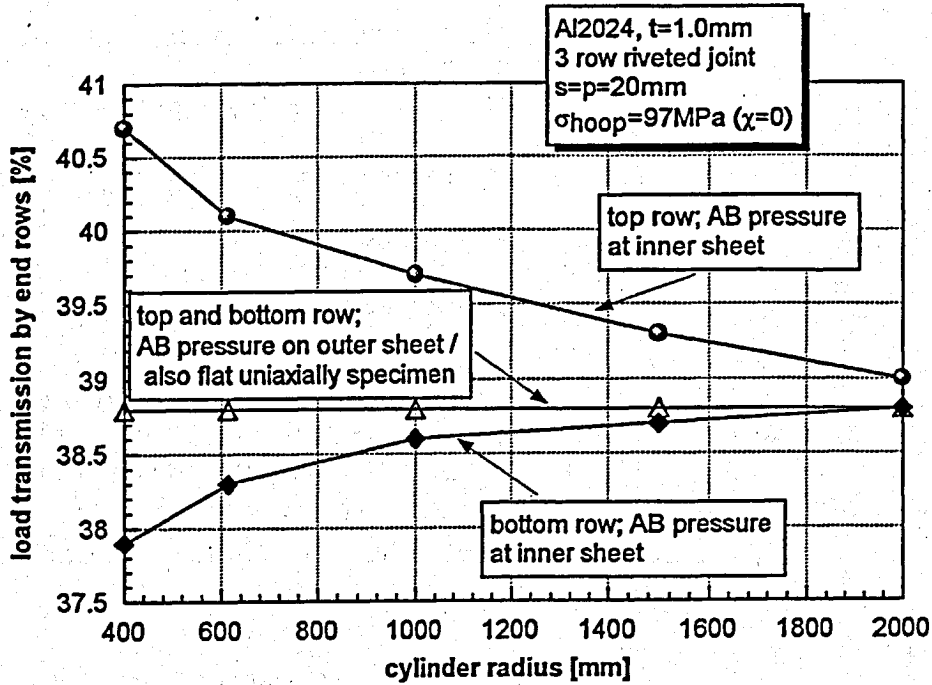
(b) Secondary bending at the critical end rows.
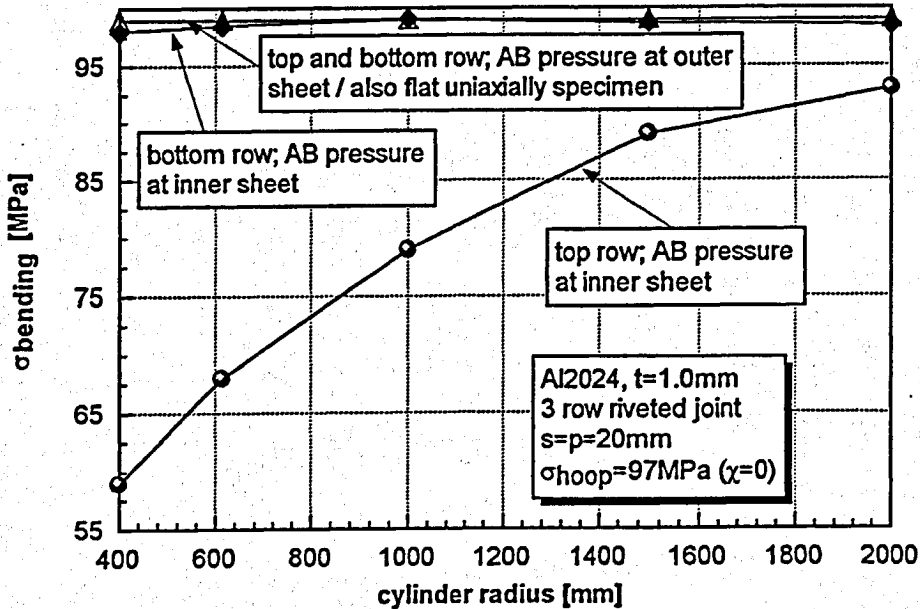
Figure 3.7   *Load transmission by the critical end rows of a riveted lap joint in unstiffened cylinders with different radii according to 2d-calculations. Two models are investigated: (1) with pressure on the free edge of the inner sheet, (2) with pressure not on the free edge of the inner sheet, but on the outer sheet [ref. 3].*
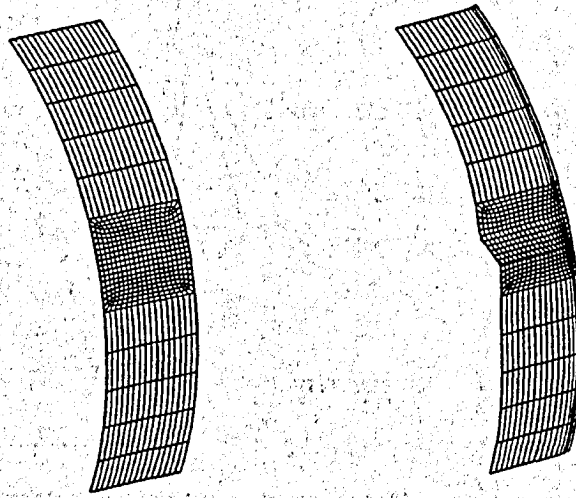
Figure 3.8 *FE mesh for a half-bay of a fuselage skin with a riveted lap joint and frame boundary conditions. Undeformed (left) and deformed (right) with: 3-rows, 613 mm radius, 400 mm width, rivet pitch (= row pitch) is 20 mm, hoop stress 97 MPa, biaxiality ratio 0.5 [ref. 3].*
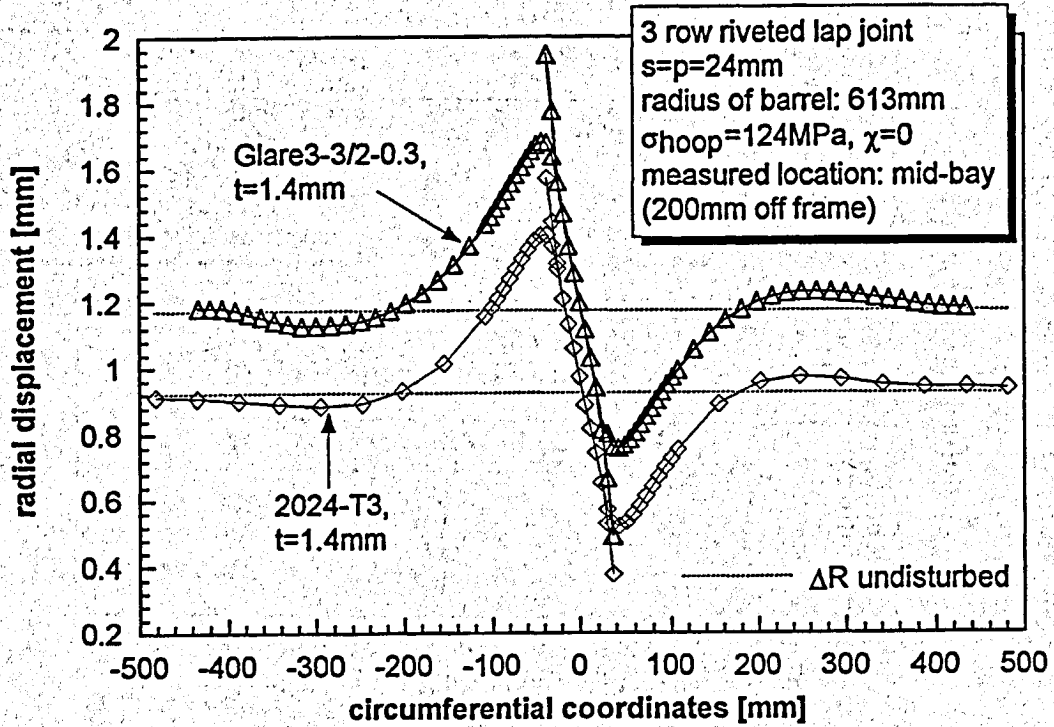
Figure 3.9 *Radial displacements of 2024-T3 and GLARE 3 lap joints midway between the rigid frames according to 3-d finite element calculations [ref. 3].*
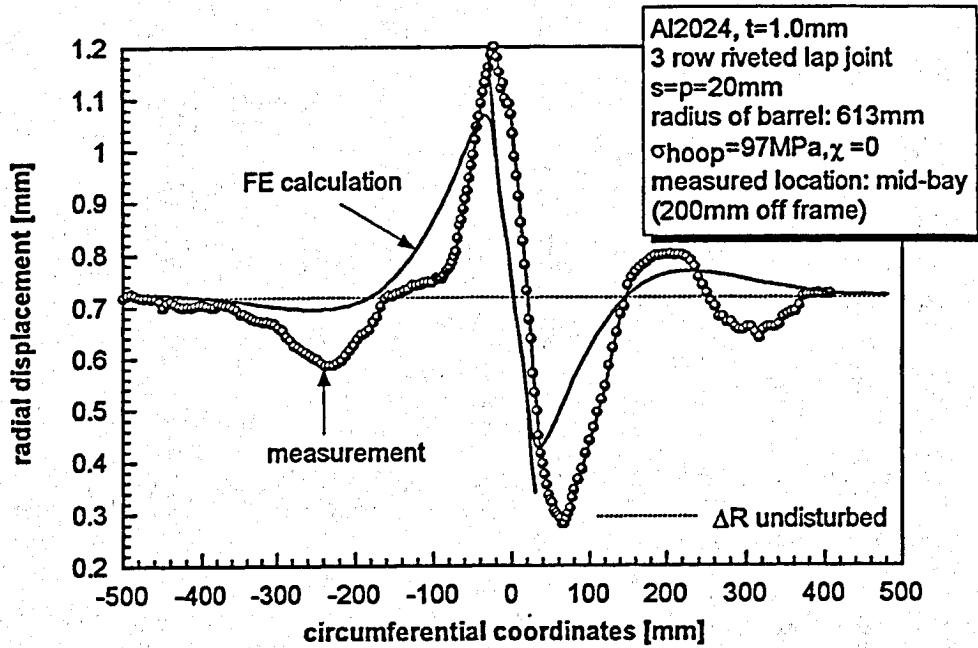
Figure 3.10 *Calculated and measured displacements of the pressurized skin in the reduced-scale barrel with a riveted joint [ref. 3].*
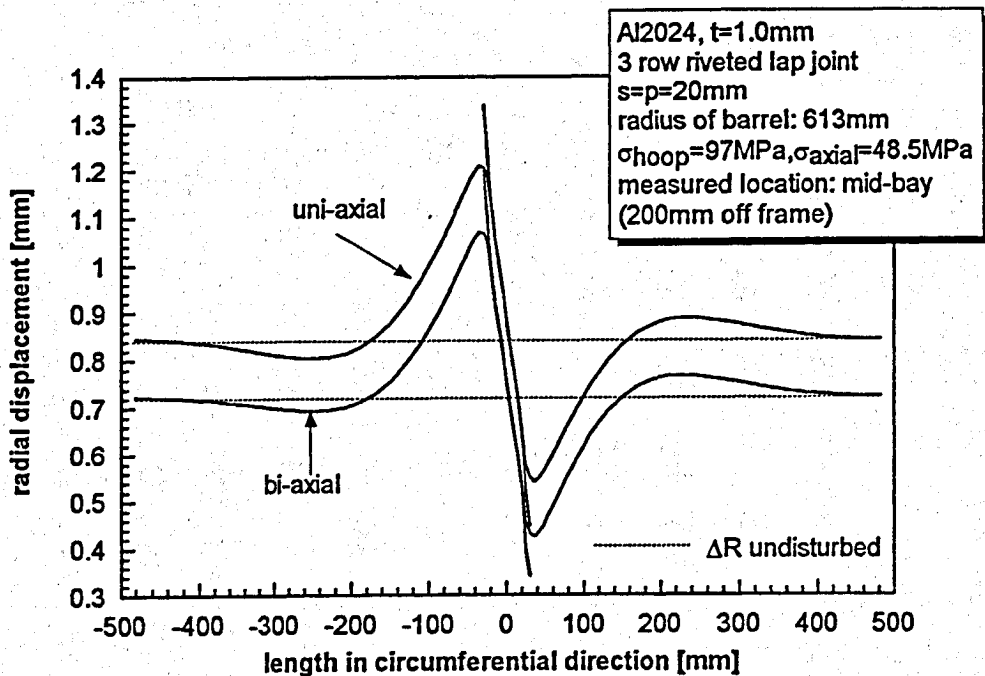
Figure 3.11 *Radial displacements of a riveted lap joint in a pressurized cylinder with rigid bulkheads. Deformations are plotted at the undisturbed location midway between the bulkheads [ref. 3].*
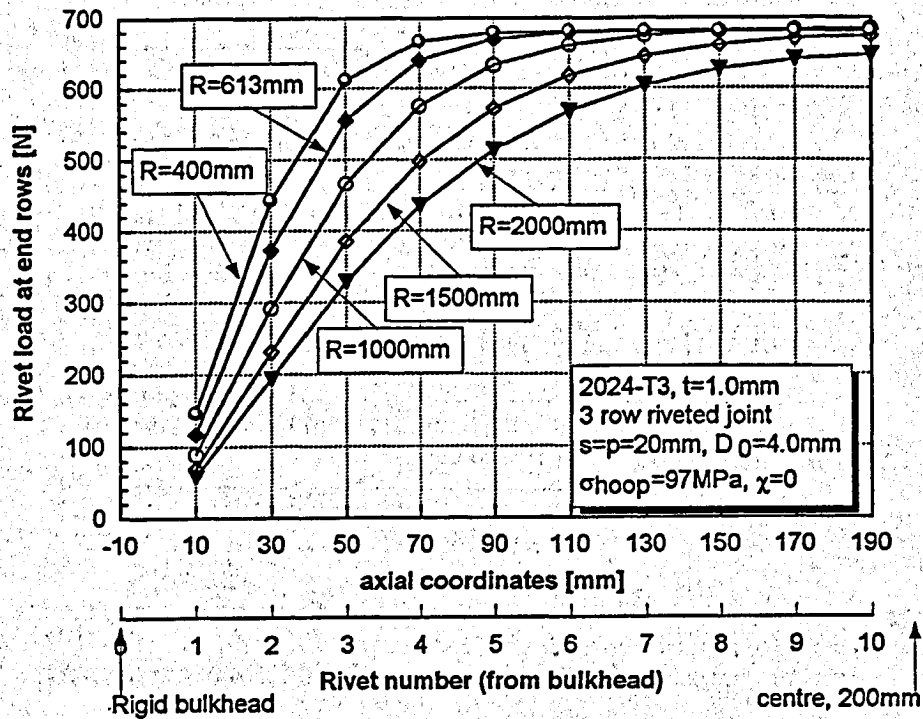
Figure 3.12a *Effect of the radius of curvature for the rivet load distribution in a riveted lap joint midway between rigid bulkheads according to 3d-FE calculations [ref. 3].*
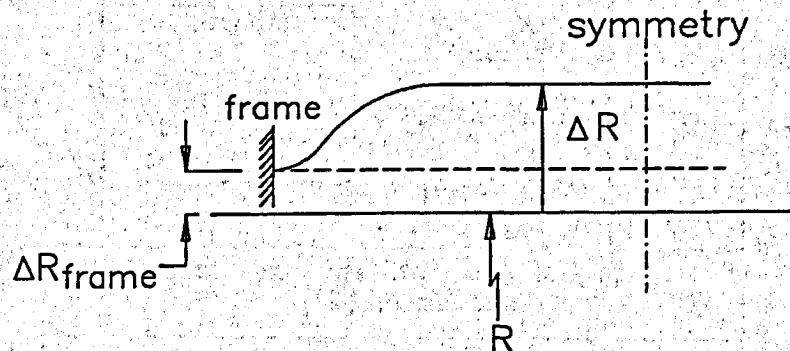
Figure 3.12b *Definitions used with for the radial displacement of frame and skin in the 3-d FE calculation. Boundary conditions at frame: all displacements besides ΔR prevented (ΔR coupled with MPC [ref. 8]) and all rotations prevented [ref. 3].*

Figure 3.12 - continued   **Memorandum M-721**

Radius of fuselage R=613mm

2024-T3,t=1.0mm,
E=70000MPa
3 row riveted joint, ·
rivet diameter: D_0=4mm
s=p=20mm
σ_{hoop} =97MPa,χ=0.5

$\Delta R_{frame}/\Delta R$=0

$\Delta R_{frame}/\Delta R$=0.33

$\Delta R_{frame}/\Delta R$=0.66

$\Delta R_{frame}/\Delta R$=1.0

FRAME   Rivet number (from frame)   MID-BAY
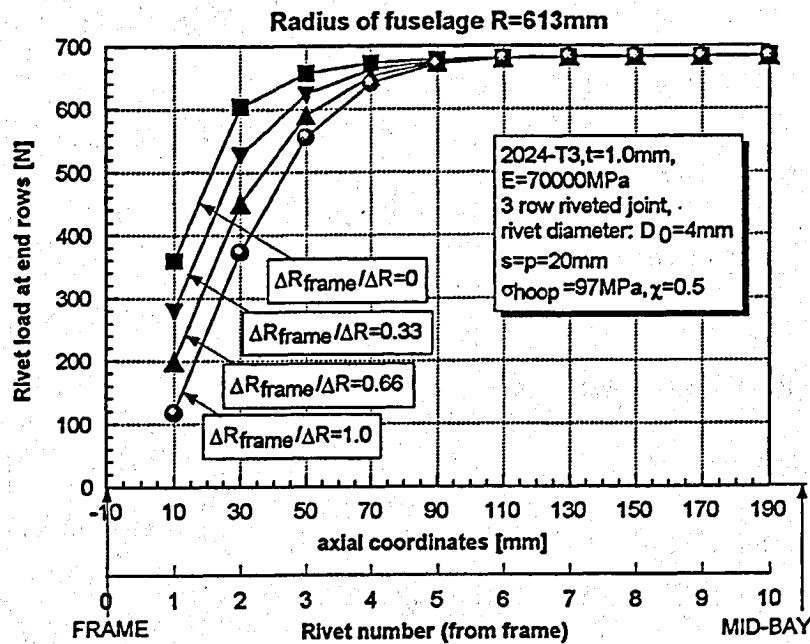
Figure 3.12c *The effect of frame stiffness for the rivet load distribution along the frame pitch. Radius of fuselage R=613mm. FE-calculation with $\Delta R_{frame}/\Delta R$ = 0, $^1/_3$, $^2/_3$, 1: frame transfers respectively 15.2% , 12.6%, 10% and 7.5% of the hoop force [ref. 3].*

Radius of fuselage R=2000mm

$\Delta R_{frame}/\Delta R$=0.66

2024-T3,t=1.0mm,
E=70000 MPa
3 row riveted joint,
rivet diameter: D_0=4mm
s=p=20mm
σ_{hoop} =97MPa,χ=0.5

$\Delta R_{frame}/\Delta R$=0

FRAME   Rivet number (from frame)   MID-BAY
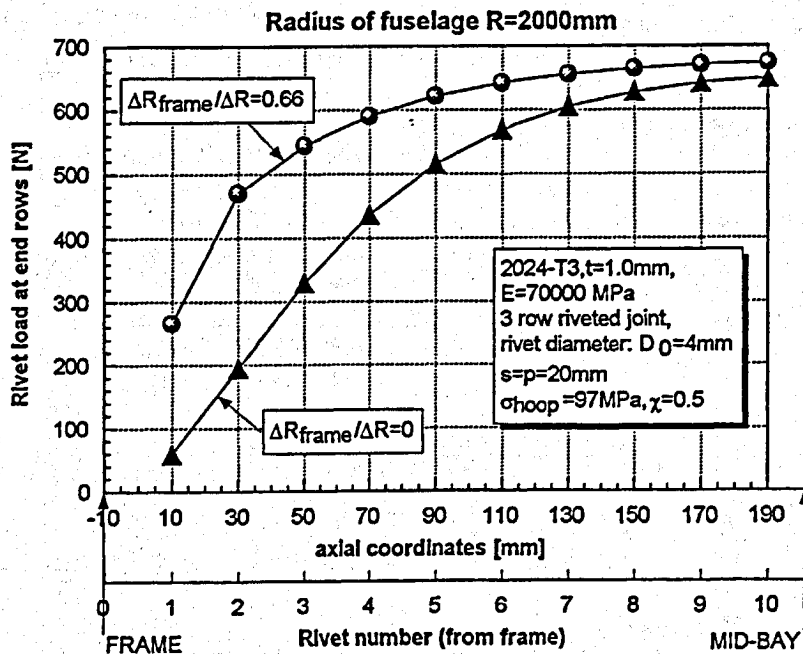
Figure 3.12d *The effect of frame stiffness for the rivet load distribution along the frame pitch. Radius of fuselage R=2000mm. FE-calculation. With $\Delta R_{frame}/\Delta R$ =0 and $^2/_3$: frame transfers 31.5% respectively 15.9% of the hoop force [ref. 3].*
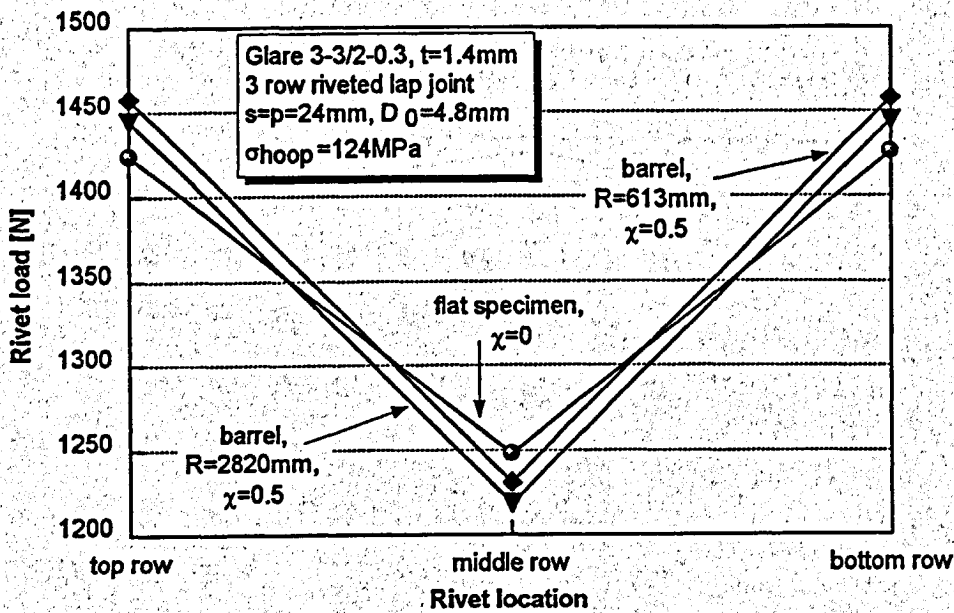
Figure 3.13 *Rivet load distribution in GLARE3 riveted lap joints according to FE calculation for flat sheets and barrel specimens midway between the frames [ref. 3].*
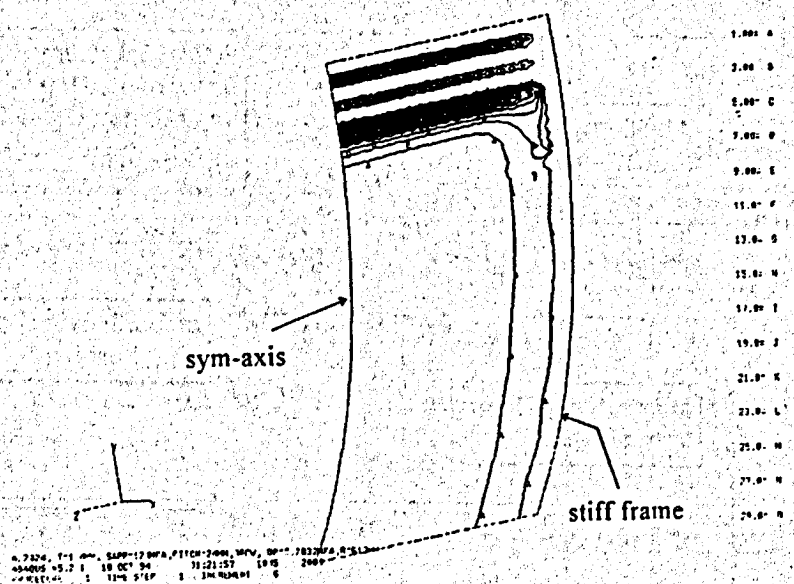
Figure 3.14 *Section moments around the longitudinal axis according to FE-calculations. Left hand side : symmetry axis, right hand side: stiff frame. Configuration: 2024-T3, t = 1.4 mm, s = p = 24 mm, D_0= 4.8 mm, Δp = 0.283 MPa, χ = 0.5 [ref. 3].*
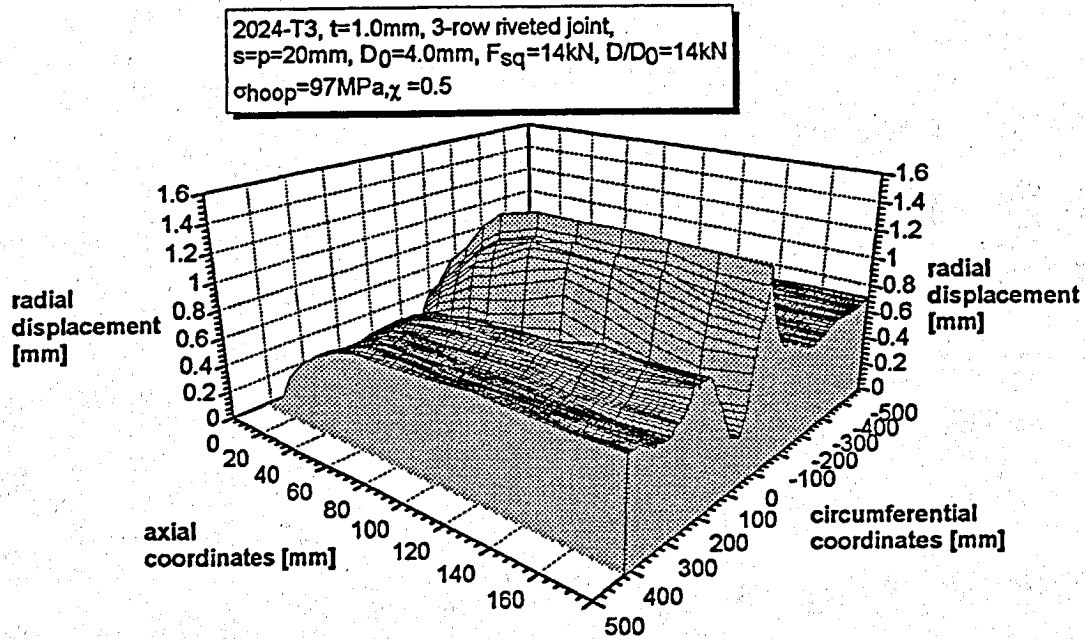
Figure 3.15a *Surface plot of measured radial displacements of a riveted lap joint in a reduced scale barrel test (elastically bent 2024-T3 sheets) [ref. 3].*
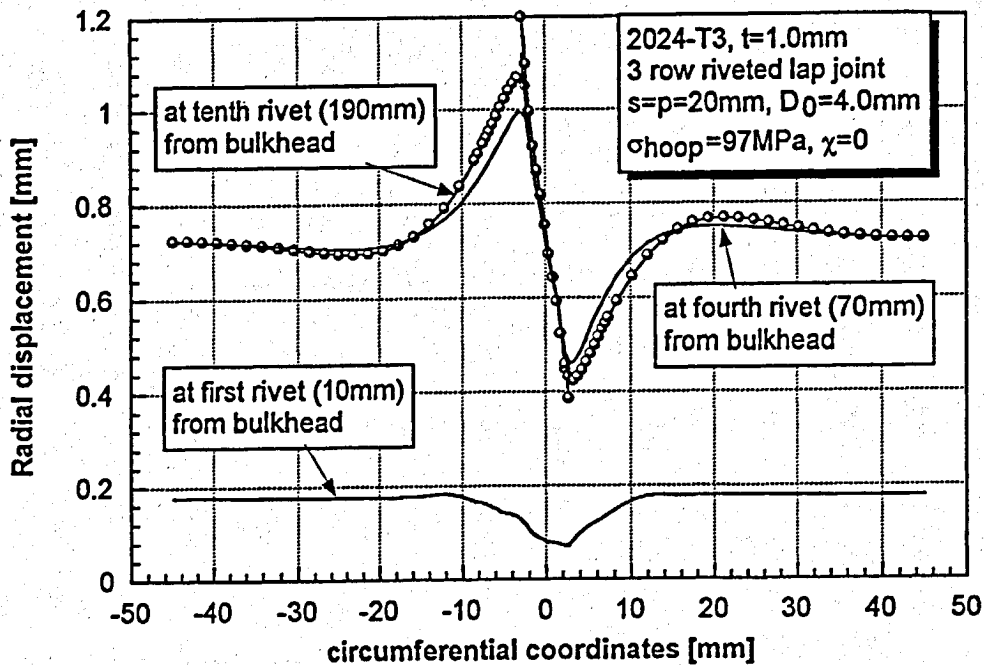
Figure 3.15b *Radial displacements and rotation of the overlap at different location removed from the rigid bulkhead according to FE-calculations [ref. 3].*
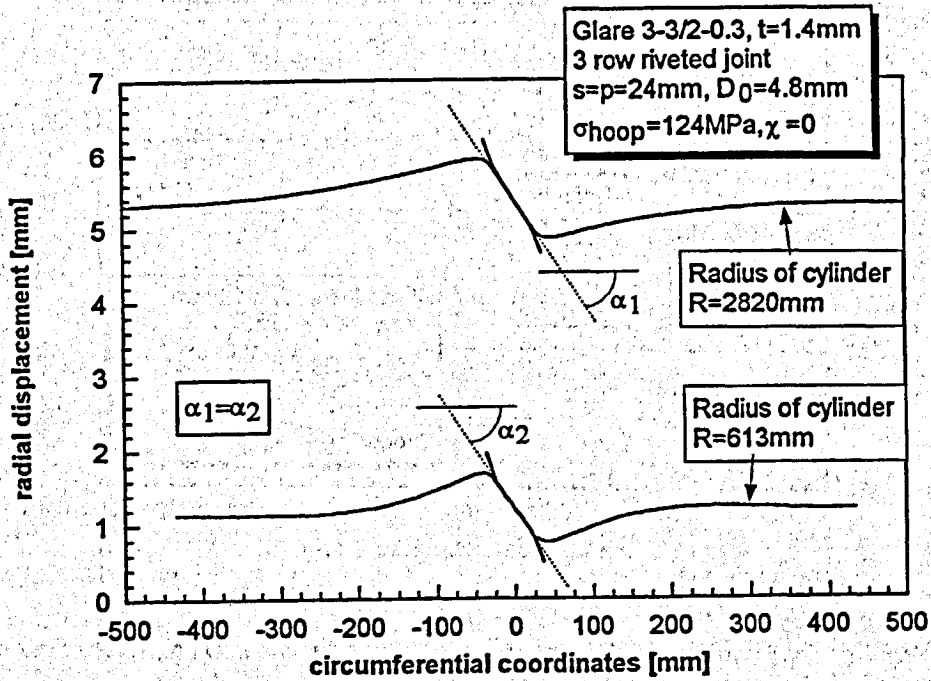
Figure 3.15c *Radial displacements midway between the bulkheads, which results in similar overlap rotations on reduced- and full-scale pressurized barrels [ref. 3].*
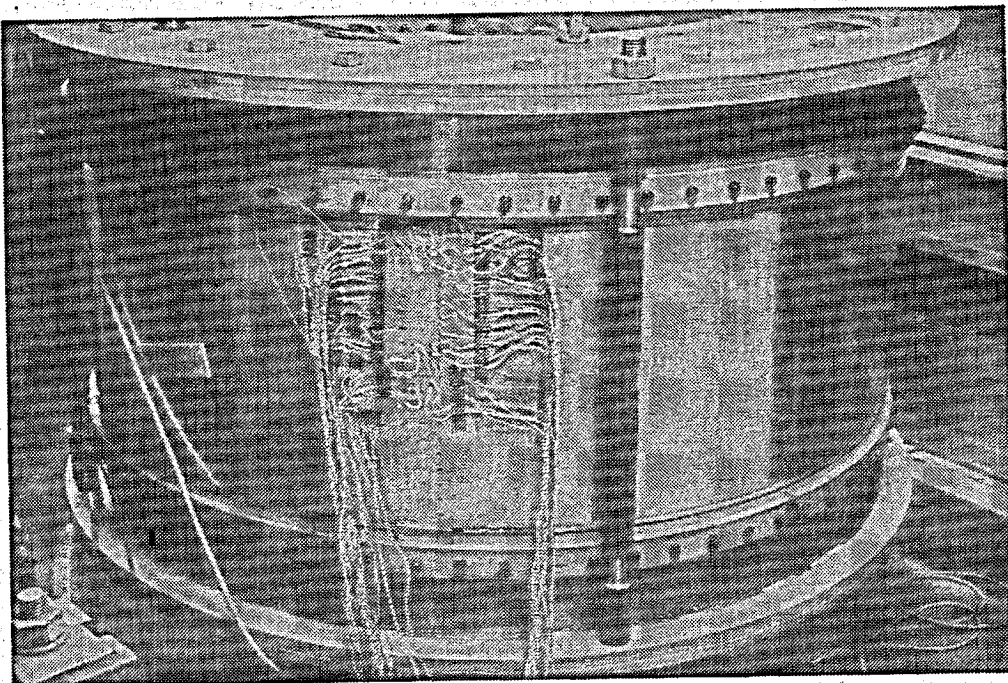
Figure 3.16 *Reduced-scale barrel specimen with strain gauges bonded close to the rivets, on the mating surfaces and the outer surfaces of the sheets [ref. 3].*
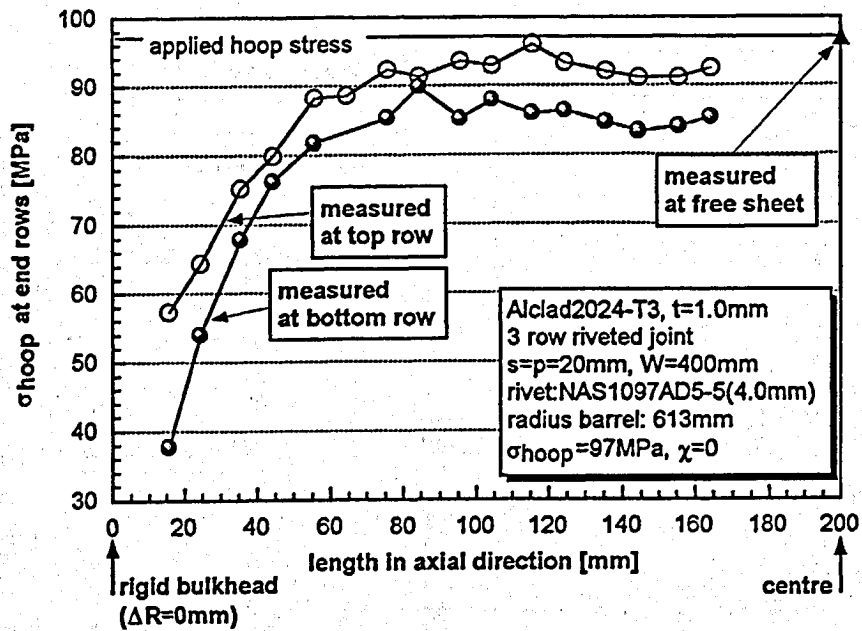
Figure 3.17 *Stresses in circumferential direction, measured near the end row rivet midway between the frames [ref. 3].*
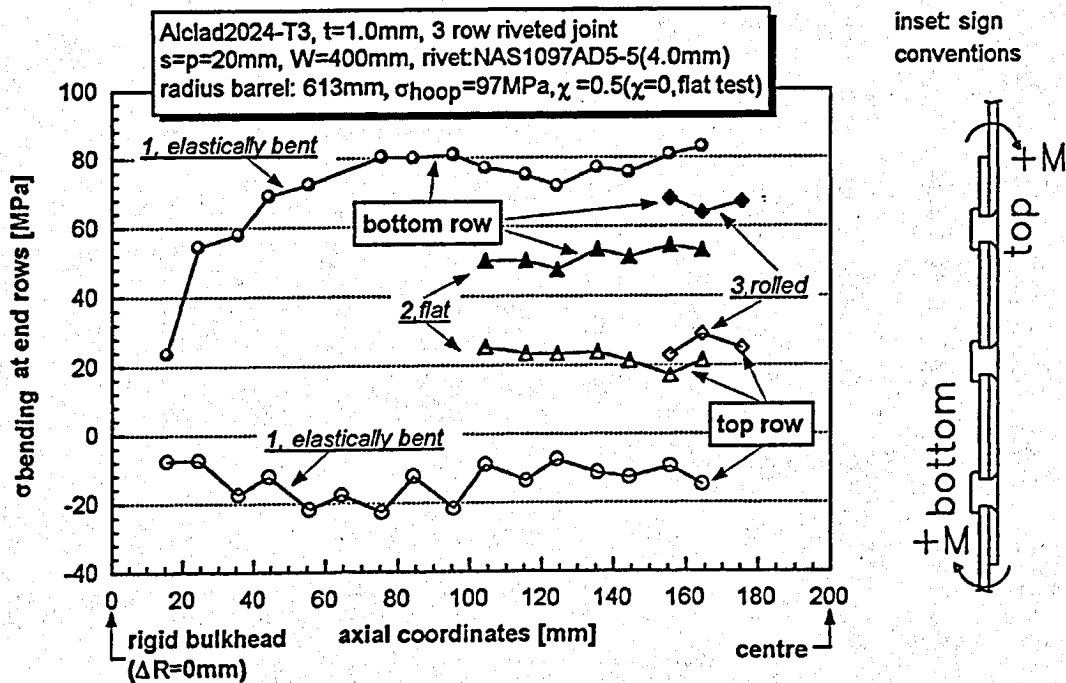
Figure 3.18 *Three secondary bending stress measurements on two different test specimens at $\sigma_{hoop} = 97$ MPa (inset: sign conventions) [ref. 3]:*

Test 1:   *Lap joint elastically curved in reduced-scale barrel test set-up.*
Test 2:   *Specimen from test 1 loaded uni-axially flat.*
Test 3:   *Lap joint of rolled sheet in reduced-scale barrel test set-up.*

Figure 3.19

(a) Top row
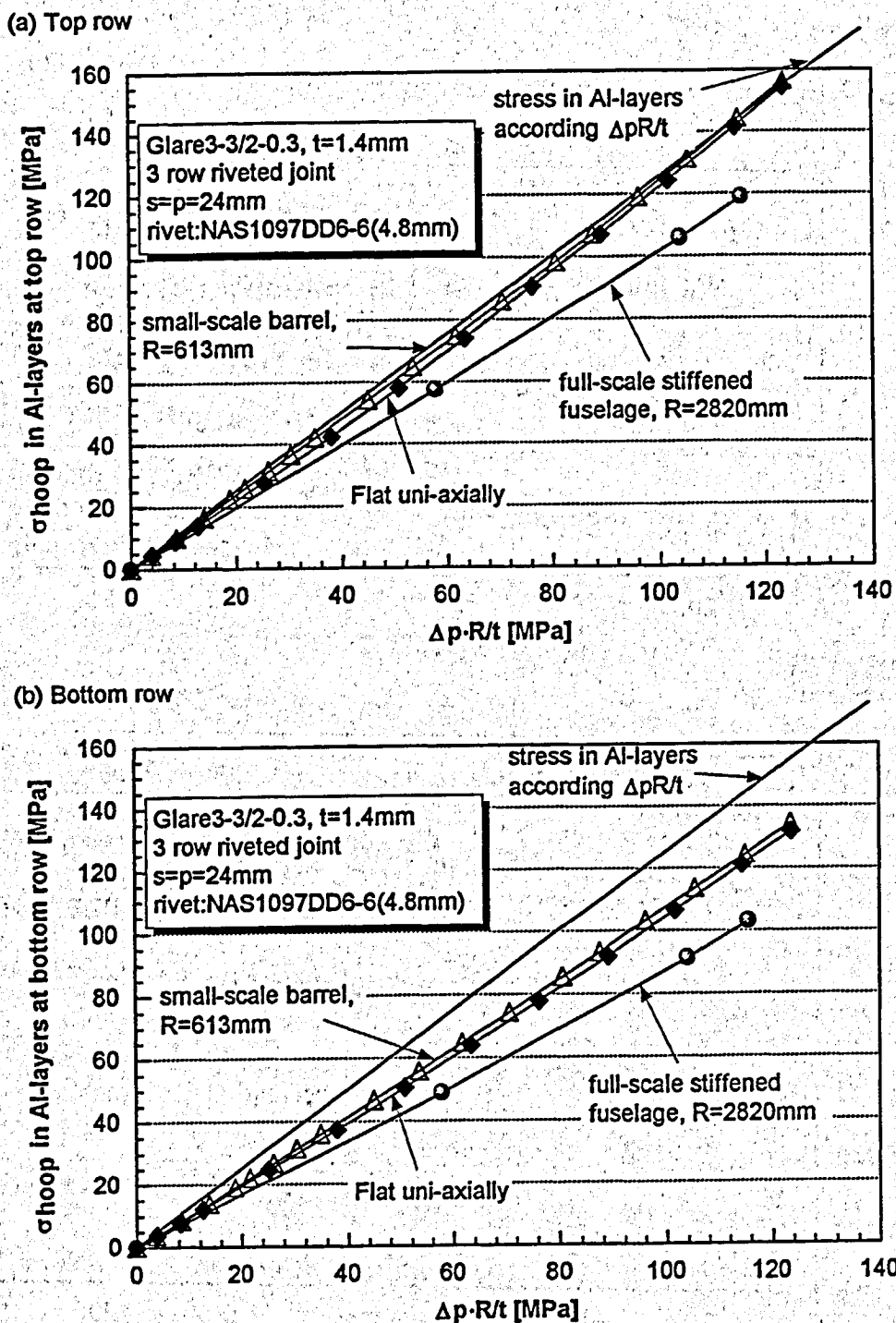
(b) Bottom row

Figure 3.19 *Stresses in the circumferential direction in the aluminium layers of the GLARE sheet. The stresses were measured near a rivet hole of the top row and the bottom row at the centre of the flat specimen, or at the midbay position of the reduced-scale barrel and the full-scale stiffened fuselage [ref. 3].*

Figure 3.20

Memorandum M-721
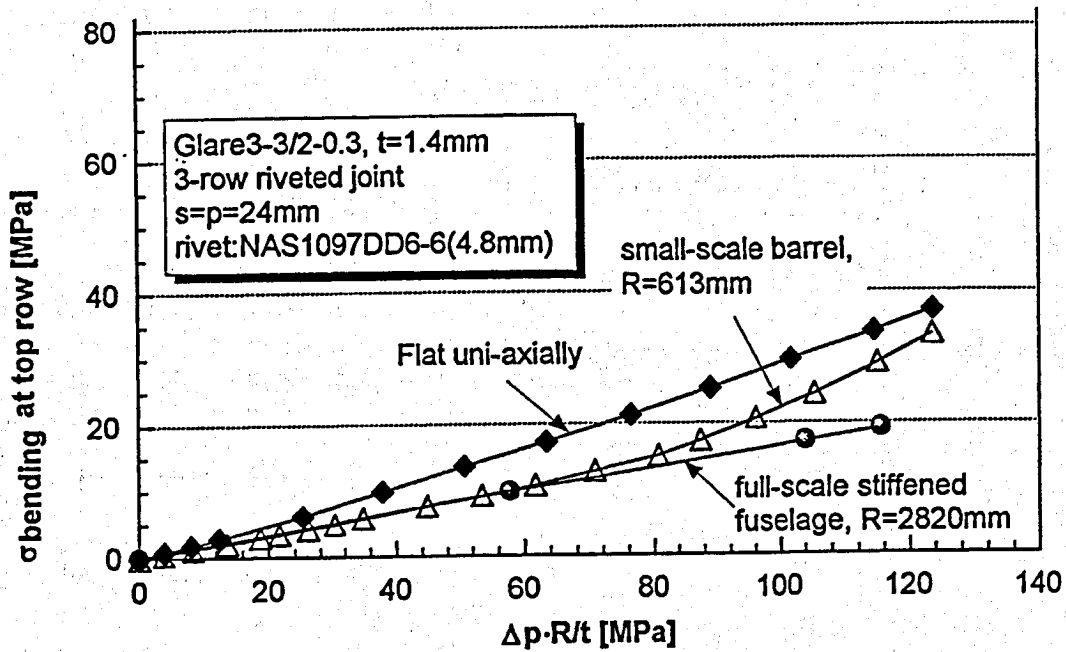
(a) Top row
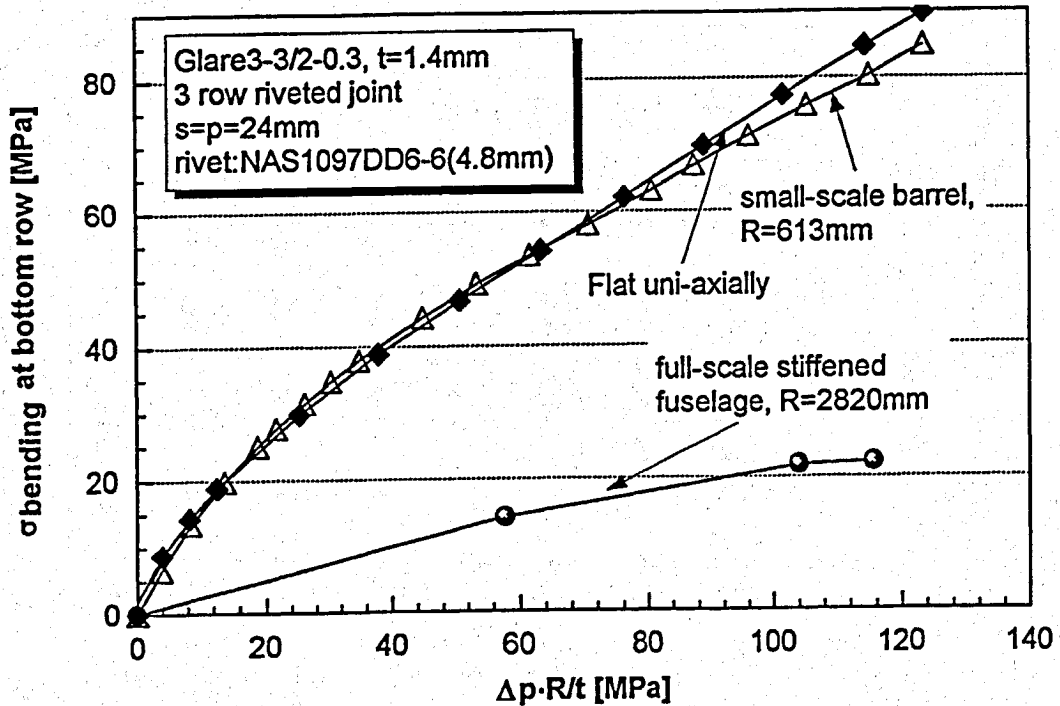
(b) Bottom row

Figure 3.20 *Bending stresses measured near a rivet of the top row and the bottom row at the centre of the flat specimen ($\chi=0$), or at the midbay position of the reduced-scale barrel and the full-scale stiffened fuselage. Results as a function of $\Delta pR/t$ [ref. 3].*

(a) Top row
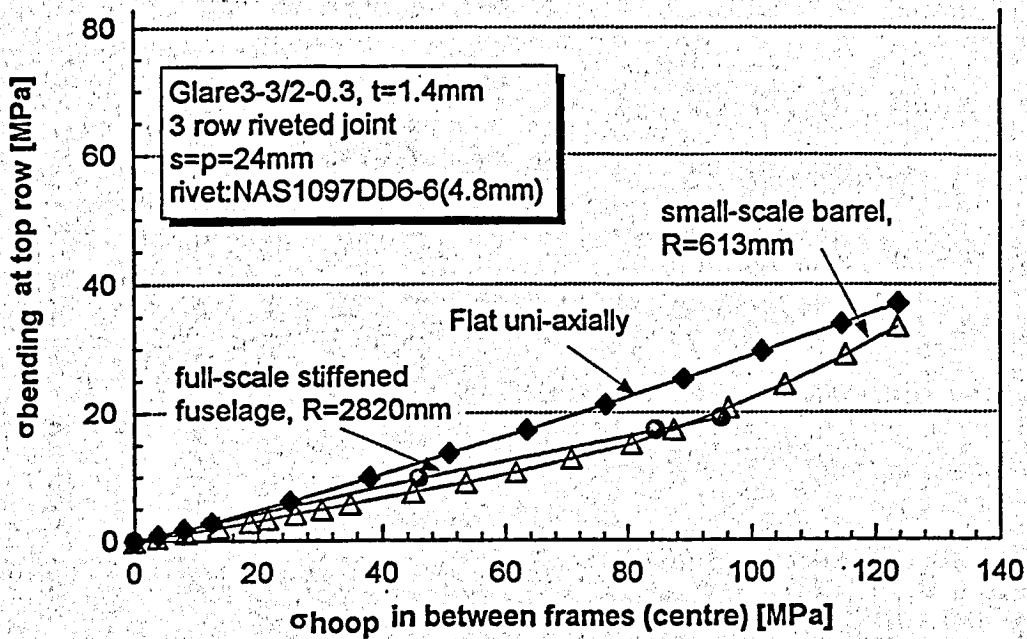
(b) Bottom row
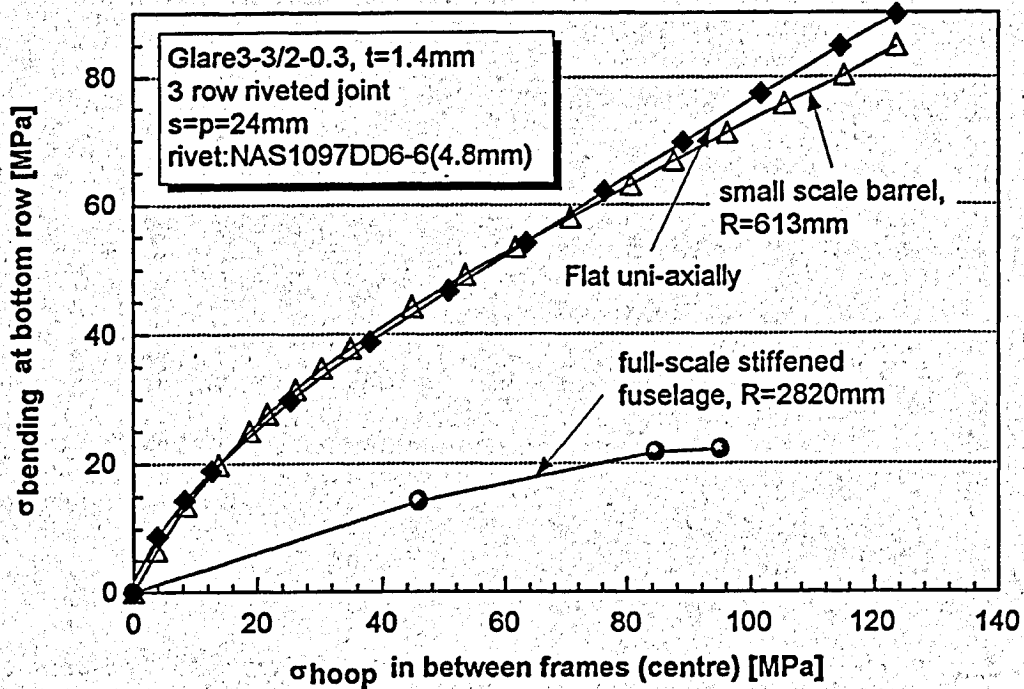
Figure 3.21 *Bending stresses measured near a rivet of the top row and the bottom row at the centre of the flat specimen, or at the midbay position of the reduced-scale barrel and the full-scale stiffened fuselage. Results as a function of the measured midbay circumferential stress [ref. 3].*

Figure 3.22   Memorandum M-721
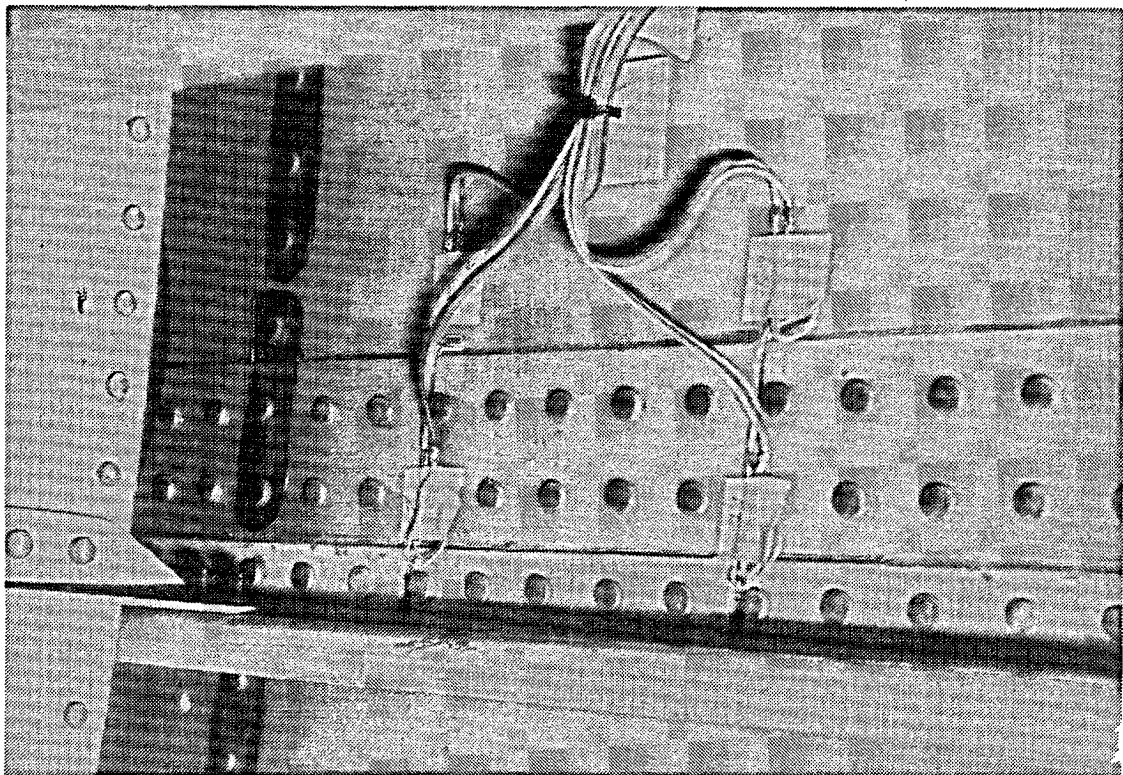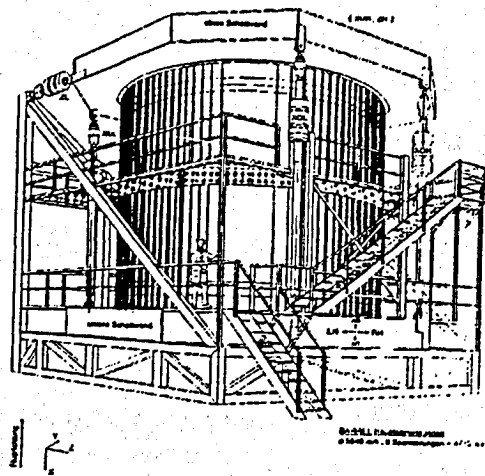
Figure 3.22 *Riveted lap joint including stiffener attachment in the Airbus A340 full-scale barrel [ref. 3].*
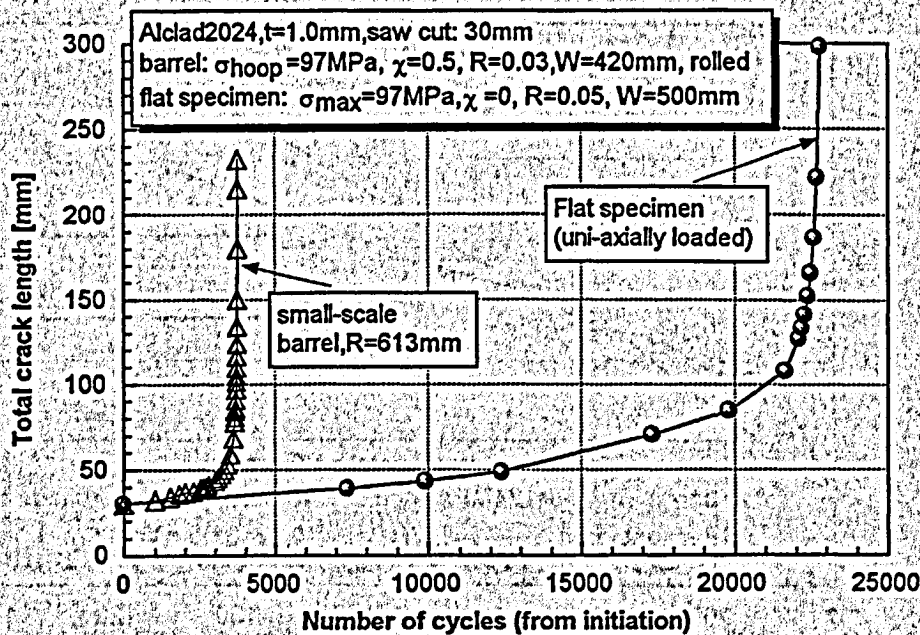
Figure 4.1 Crack growth in the free sheet of the reduced-scale barrel test set-up, and in a flat sheet specimen. Material: 1.0 mm 2024-T3. Cracks started from a saw cut [ref. 3].
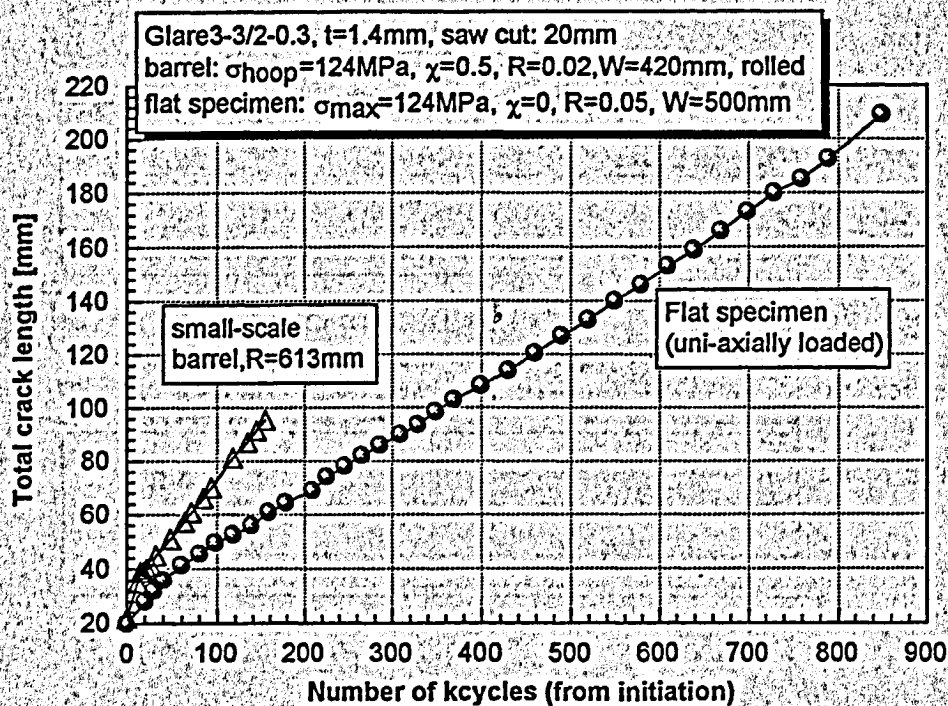
Figure 4.2 Crack growth in the free sheet of the reduced-scale barrel test set-up, and in a flat sheet specimen. Material: GLARE3-3/2-0.3, t = 1.4 mm. Cracks started from a saw cut [ref. 3].
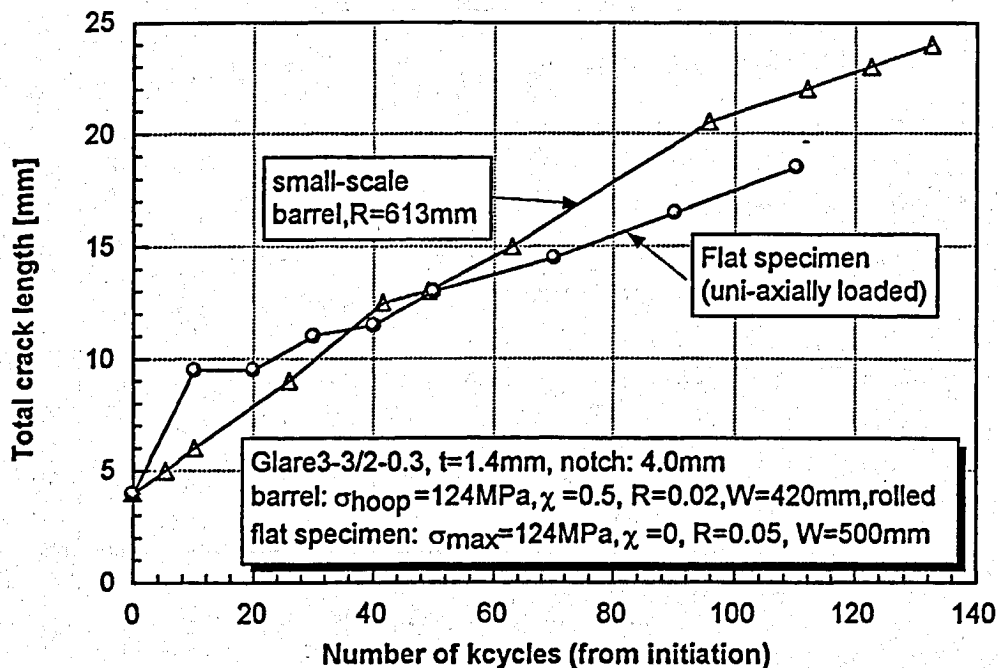
Figure 4.3 *Crack growth in the free sheet of the reduced-scale barrel test set-up, and in a flat sheet specimen. Material: GLARE3-3/2-0.3, t = 1.4 mm. Cracks started from a notch, diameter 4.0 mm [ref. 3].*
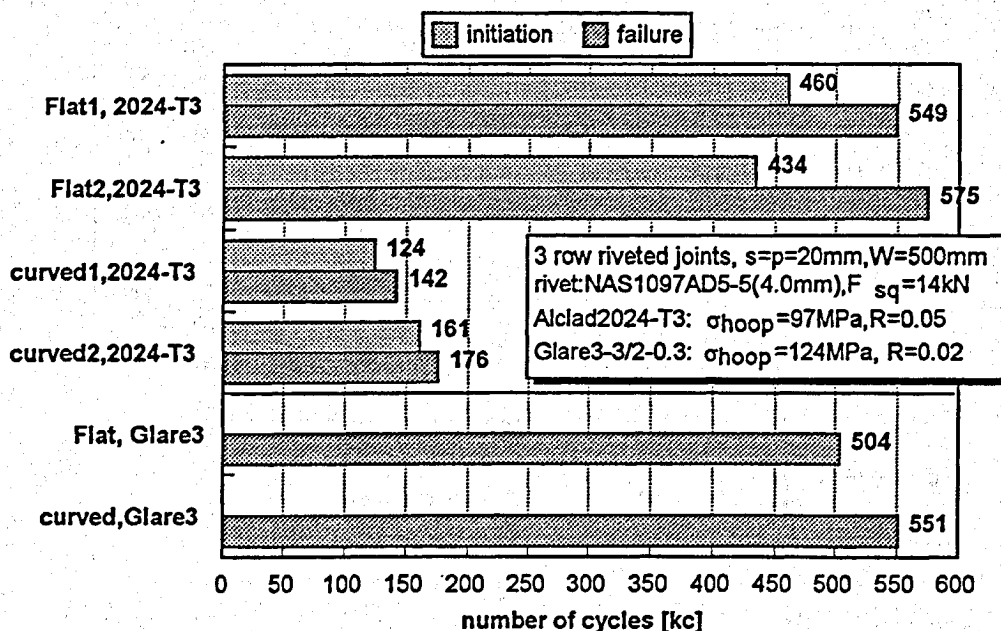
Figure 4.4 *Fatigue crack initiation ($\cong$1mm) and failure of uniaxially loaded flat and curved riveted lap joint specimens. The curved specimens (R=2000 mm) are loaded by internal pressure (χ=0 [ref. 3].*
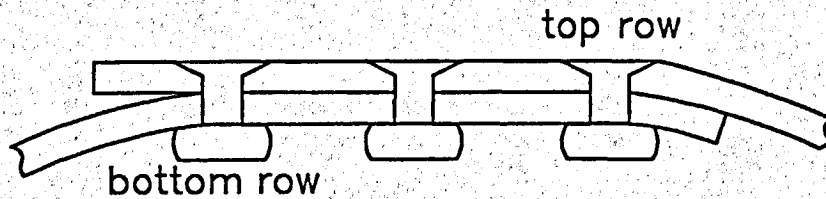
Figure 4.5 *Initial deformation induced by elastic bending of a riveted lap joint of non-roll formed sheets [ref.3].*
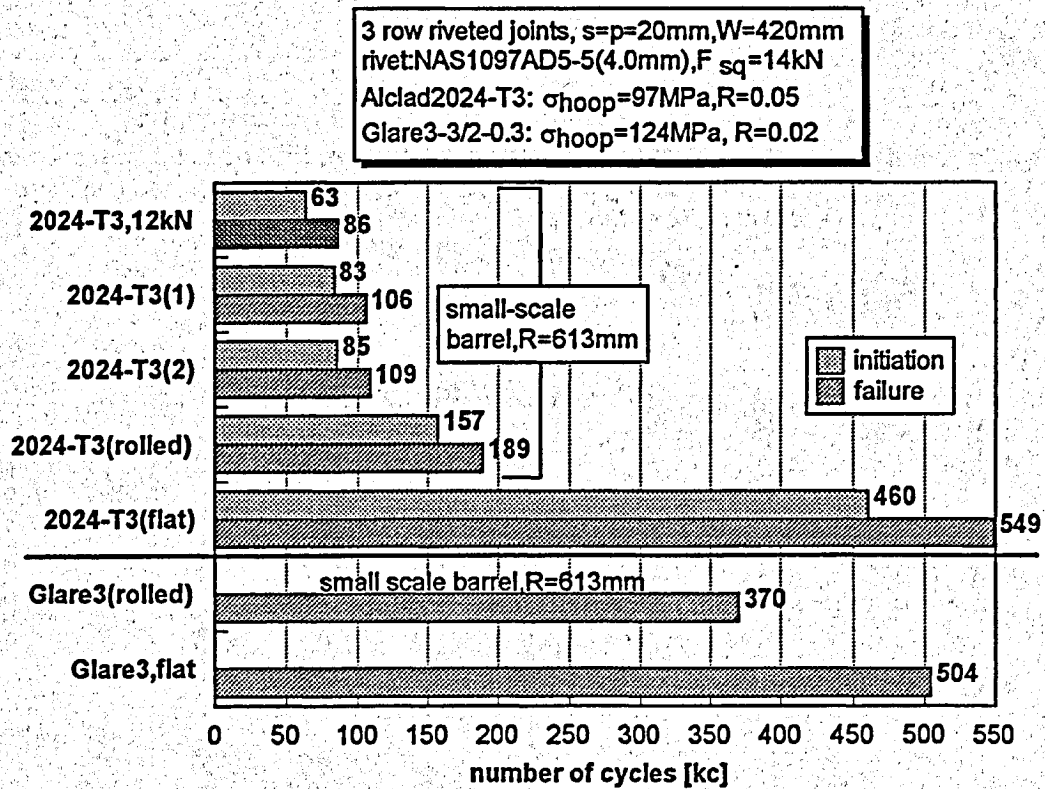
Figure 4.6 *Fatigue crack initiation (≤1mm) and failure of riveted lap joints of 2024-T3 (t = 1.0 mm) and GLARE 3-3/2-0.3 (t = 1.4 mm) tested in the reduced-scale barrel test set up. Comparison to uniaxially loaded flat specimen results [ref. 3].*

Figure 4.7

Memorandum M-721
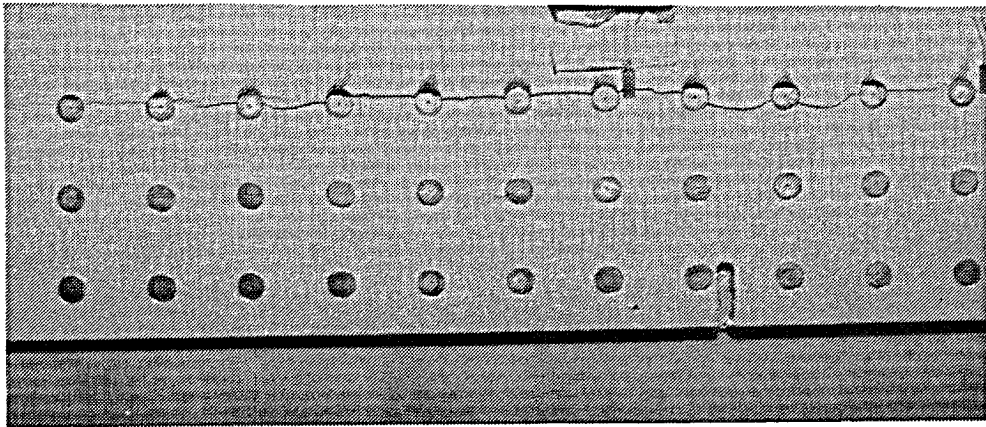
Figure 4.7a *Fatigue cracks in top row of riveted lap joint of a reduced-scale barrel specimen with σ_{hoop}=124MPa. Configuration: GLARE3-3/2-0.3, 3-row riveted joint, s=p=20 mm, D_0 = 4.0 mm. F_{sq}=14kN [ref. 3].*
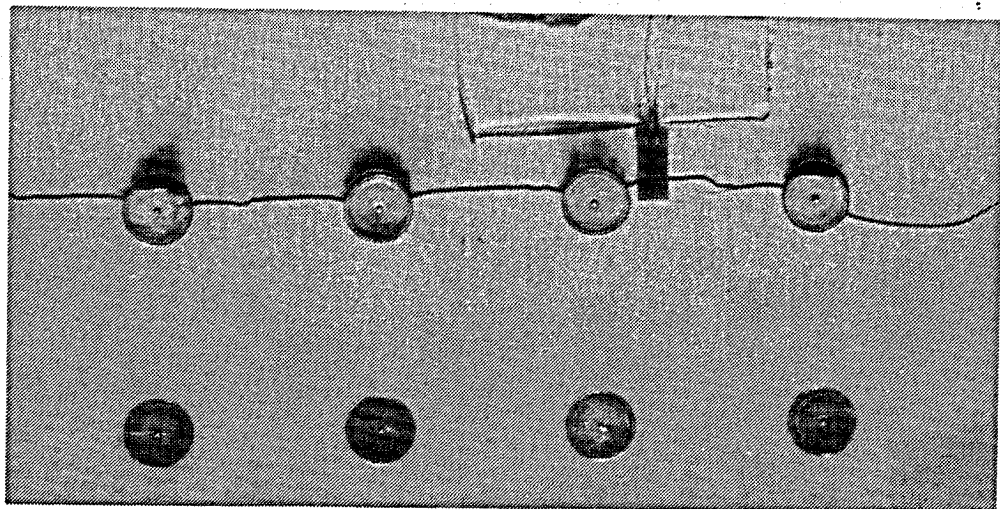
Figure 4.7b *Close up of figure 3.29a [ref. 3].*

(a) Top row
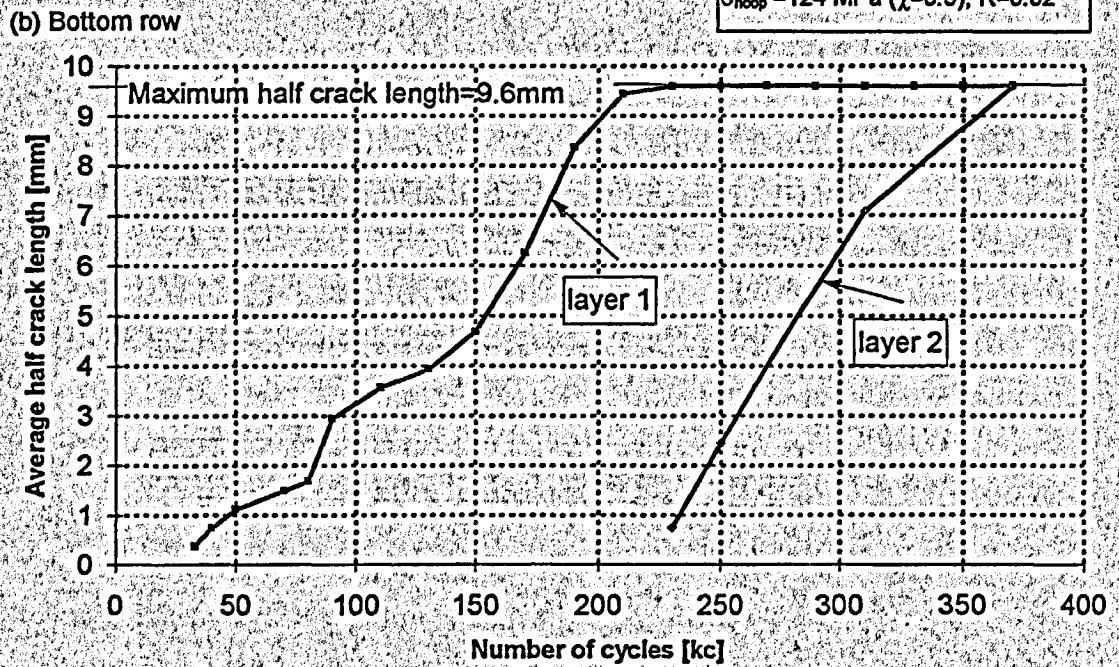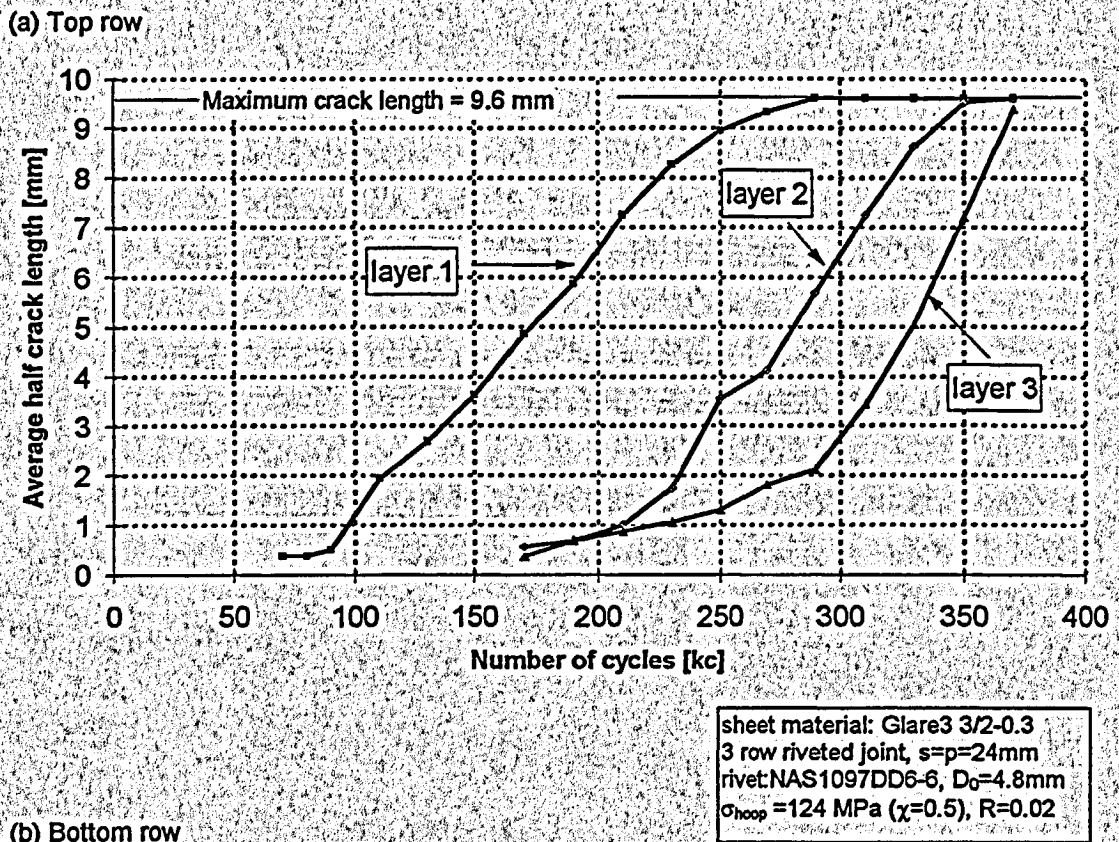

(b) Bottom row

sheet material: Glare3 3/2-0.3
3 row riveted joint, s=p=24mm
rivet:NAS1097DD6-6, D_0=4.8mm
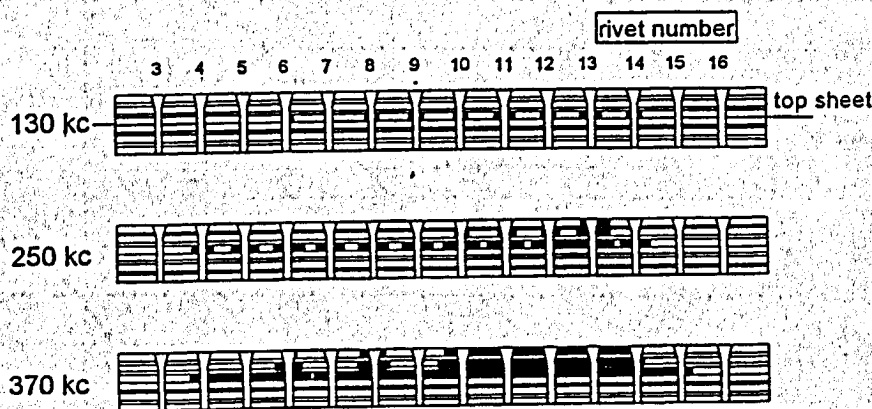σ_{hoop} =124 MPa (χ=0.5), R=0.02

Figure 4.8 *Crack growth in the top row and the bottom row of the lap joint in the reduced-scale barrel test set-up. Results of rivets 4 to 15, unaffected by bulkheads [ref. 3].*
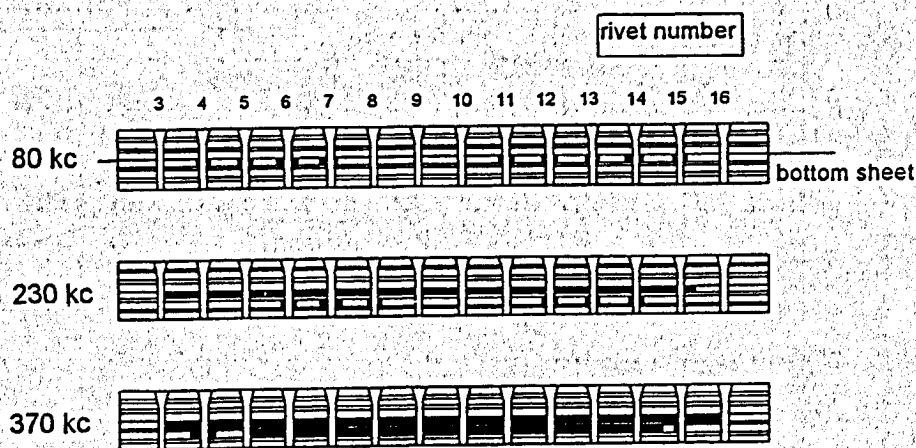
(c) MSD in top row

(d) MSD in bottom row

Figure 4.8 Continued. Crack length in the top row and bottom row of the riveted joint at different numbers of cycles [ref. 3].
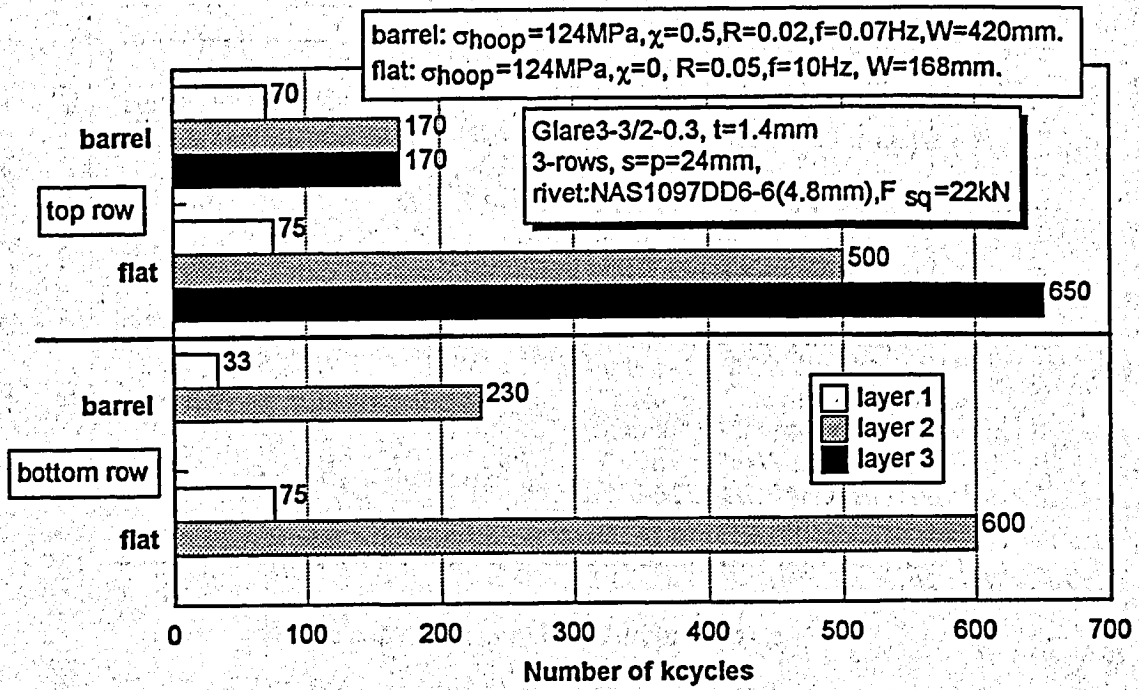
barrel: σhoop=124MPa, χ=0.5, R=0.02, f=0.07Hz, W=420mm.
flat: σhoop=124MPa, χ=0, R=0.05, f=10Hz, W=168mm.

Glare3-3/2-0.3, t=1.4mm
3-rows, s=p=24mm,
rivet:NAS1097DD6-6(4.8mm), F sq=22kN

Figure 4.9 *Crack initiation lives (≅1mm) of the individual layers of a GLARE riveted lap joint at the critical top row and bottom row tested in the reduced-scale barrel and an identical configuration tested as a flat uniaxially loaded specimen [ref. 3].*

Figure 4.10   Memorandum M-721

(a) Test data
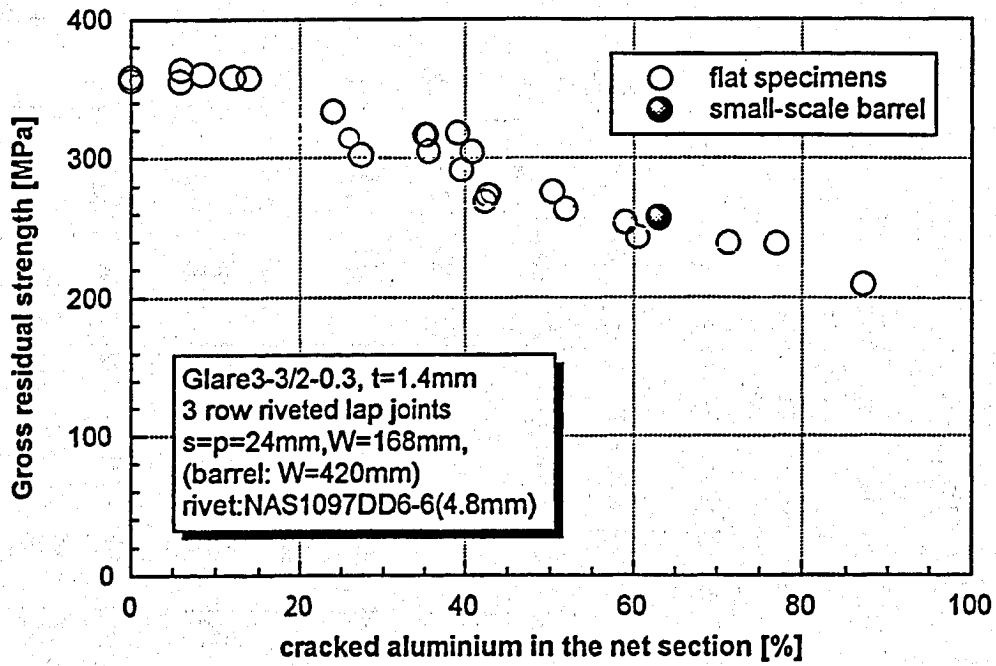
(b) Photograph of barrel after residual strength test

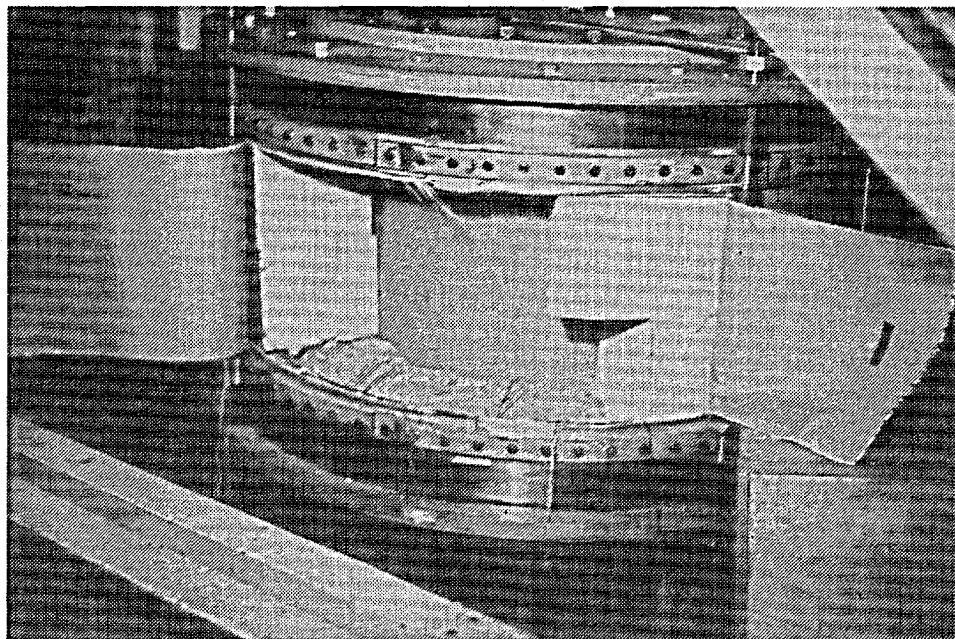**Figure 4.10** *The residual strength obtained in the reduced-scale barrel test (R=613mm, χ=0.5) on a GLARE 3 riveted lap joint, compared to results of flat GLARE 3 riveted lap joints [ref. 3].*
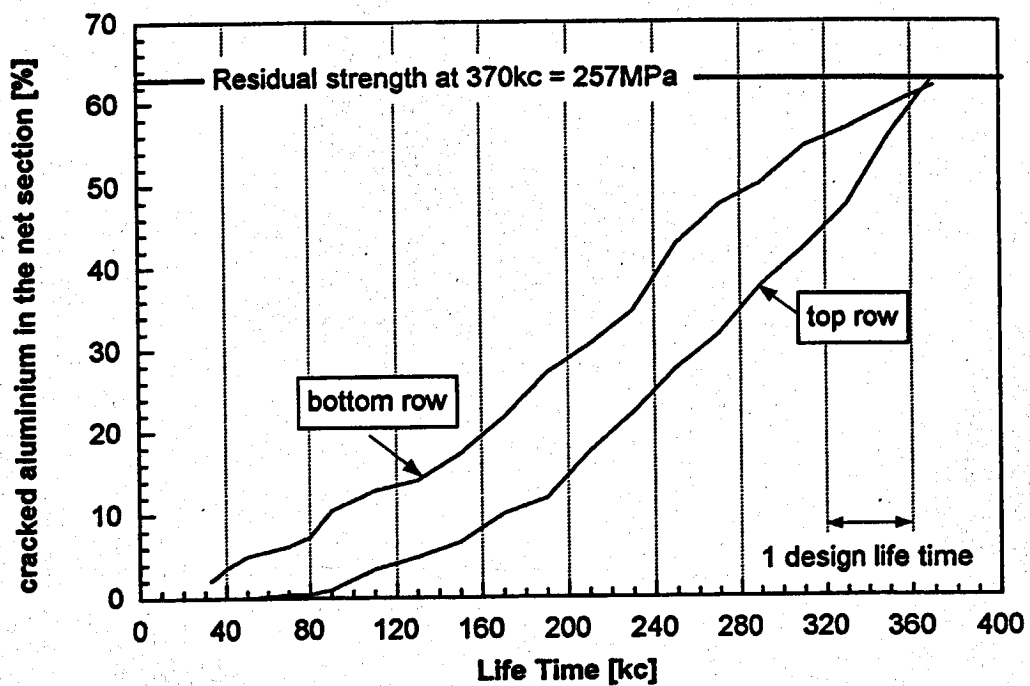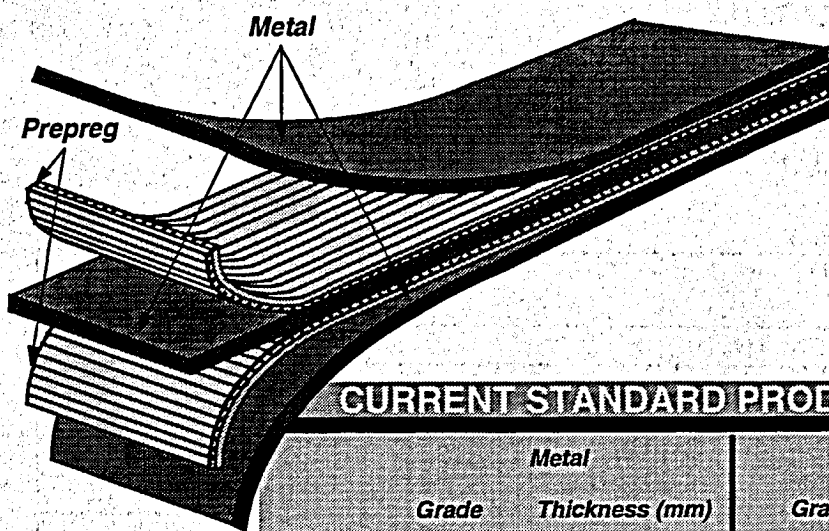
Figure 4.11   *The damage tolerance behaviour observed in the reduced-scale barrel test on a GLARE 3-3/2-0.3 specimen (t=1.4 mm) with the riveted lap joint configuration of the A340. Results of rivets 4 to 15, unaffected by bulkheads [ref. 3].*

LEFT BLANK INTENTIONALLY

APPENDIX A   GLARE STANDARD CONFIGURATIONS

GLARE 3 3/2 lay-up (schematic)

CURRENT STANDARD PRODUCT FORMS

	Metal		Prepreg	
	Grade	Thickness (mm)	Grade	Thickness (mm)
GLARE 1	7475-T761	0.3 - 0.4	U.D. glass	0.25
GLARE 2	2024-T3	0.2 - 0.3 - 0.4	U.D. glass	0.25
GLARE 3	2024-T3	0.2 - 0.3 - 0.4	C.P. glass 50/50	0.25
GLARE 4	2024-T3	0.2 - 0.3 - 0.4	C.P. glass 67/33	0.375
GLARE 5	2024-T3	0.2 - 0.3 - 0.4	C.P. glass 50/50	0.5

U.D. = unidirectional; C.P. = cross-ply;

50/50 = 50 % of fibres in longitudinal direction and 50 % in long-transverse direction;

67/33 = 67 % of fibres in longitudinal direction and 33 % in long-transverse direction.
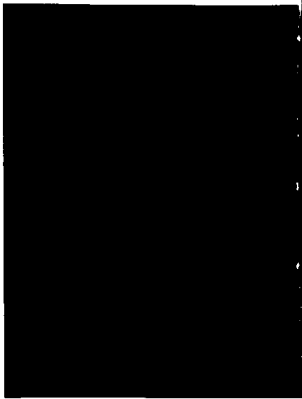
GLARE classification

GLARE A-B/C-D   A = GLARE grade;
                  B = number of aluminium layers
                  C = number of fibre/adhesive layers
                  D = nominal thickness of individual aluminium layer in mm
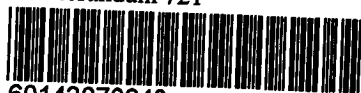
APPENDIX B

Radial deflections of the inner sheet and outer sheet of a riveted lap joint 40° removed from the lap joint in a pressurized cylinder according 2-d FE (χ=0) calculations (in comparison with theoretical radial displacements of unstiffened pressurized cylinders with hoop stress {[#] $\Delta R = \Delta p \cdot R^2 / (E \cdot t)$})

Material   :   2024-T3 (1.0 mm)
Lap joint   :   - 3 rivet-row
                         - NAS1097AD5-5 (4.0 mm) rivets
                         - s = p = 20 mm
Applied stress :   97 MPa

inner sheet			outer sheet			cylinder (#)
R	ΔR	R+ΔR	R	ΔR	R+ΔR	R+ΔR
299.5	0.8863	300.39	300.5	-0.1162	300.38	300.40
612.5	1.301	613.80	613.5	0.3059	613.81	613.81
999.5	1.863	1001.36	1000.5	0.8049	1001.30	1001.33
1499.5	2.475	1501.98	1500.5	1.479	1501.98	1501.99
1999.5	3.138	2002.64	2000.5	2.143	2002.64	2002.66